ISSN 0915-633X

NATIONAL INSTITUTE FOR FUSION SCIENCE

Dynamic Behavior of Hydrogen Atoms with a Boronized Wall

K. Tsuzuki, N. Inoue, A. Sagara, N. Noda, O. Motojima,
T. Mochizuki, T. Hino and T. Yamashina

(Received - June 18, 1997)

NIFS-500 July 1997

RESEARCH REPORT
NIFS Series

NAGOYA, JAPAN

TITLE

Dynamic behavior of hydrogen atoms with a boronized wall

Authors

K. Tsuzuki, N. Inoue, A. Sagara, N. Noda, O. Motojima,

[1]T. Mochizuki, [1]T. Hino, and [1]T. Yamashina.

National Institute for Fusion Science

322-6 Oroshi-cho Toki 509-52, Japan

[1]Department of nuclear engneering. Hokkaido university, Sapporo 060, Japan

Abstract

Dynamic behavior of hydrogen atoms in boron films, which is one of candidate materials of the first wall of fusion devices, has been studied. Boron films were deposited on the whole inner surface of a liner, which acts as a large test piece with a surface area of 7000 cm^2. Hydrogen absorption behavior was investigated with the glow discharge in hydrogen. After a strong absorption into the near surface region, hydrogen atoms were slowly and continuously absorbed for 10 hours without saturation. A helium glow discharge was carried out after the hydrogen discharge to investigate hydrogen desorption by the He ion bombardment. Fifteen percents of the absorbed H atoms were desorbed. The strong absorption was observed at the initial phase of the hydrogen discharge after the He discharge due to the evacuation of the H atoms from the surface during the He discharge. The number of absorbed hydrogen atoms was larger than one desorbed during the He discharge, which indicates that hydrogen atoms accumulate in the film when the H_2 and He discharges are repeated alternately. The slow absorption is due to migration of hydrogen atoms deeper into the film enhanced by the ion bombardment. Depth profile measurements with elastic recoil detection (ERD) give a consistent result. Most of the retained hydrogen atoms were released by heating up to 400 °C. A possibility of the boron films as a protection wall of tritium permeation is suggested. A calculation based on a simple model was discussed with the experimental results. A recombination coefficient was obtained through the calculation of the transient release of the H atoms just after the H_2 discharge. The time behavior at the initial phase of the He discharge was reproduced fairly well by assuming a smaller cross-section for ion induced detrapping .

Submitted to Journal of Nuclear Materials on 12 June 1997.

1. Introduction

It is known that the plasma-facing first wall in fusion devices plays an important role for impurity and fuel control. By aiming a reduction of metal impurities, and thus, radiation losses, low Z materials like carbon, boron, beryllium, and lithium have been employed in many devices and investigated for many years [1-11].

In-situ boron coating (boronization) was first applied in TEXTOR in 1989 [4]. Reduction of carbon and oxygen impurities is observed compared to the carbonized wall due to oxygen gettering ability of the boron film. Improvement in plasma performance has been achieved for most of the devices with the boronization [4-9]. In addition, hydrogen recycling from the boron film is relatively lower compared to the carbon walls [4,5]. Boronization is planned in Large Helical Device (LHD) because of the above noted merits. However one of the concerns is hydrogen behavior, especially recycling with a low temperature wall, since the baking temperature is limited less than 100 °C in LHD [12]. Thus, in this work, we focus our attention to hydrogen behavior with the boron coating films.

Understanding of the hydrogen behavior is important from a view point of fuel control when low Z materials are used, which retain a large amount of hydrogen atoms. The plasma density control becomes difficult if a considerable number of hydrogen atoms are re-emitted (recycled) from the wall because the density increases without external fuelling [13]. In addition, it is reported that low recycling condition is favorable to obtain good energy confinement [14]. The reduction of hydrogen recycling at a wall surface is considered to be an important issue for better density control and performance in the present devices.

In long time discharges, transient release of excess hydrogen atoms may take place in some conditions, which makes plasma density control difficult [15]. Understanding of dynamic behavior of the hydrogen recycling is important for better control. Tritium inventory will be a serious problem in DT burning devices. Thus it is important not only to reduce the hydrogen recycling but also to understand hydrogen behavior precisely for future devices.

It is reported that high temperature baking is effective to reduce the hydrogen recycling. In devices such as JT-60U, TEXTOR, and DIII-D, in which wall temperature can be heated up to 300 °C, the hydrogen recycling is well reduced with the boronized wall compared to the carbonized wall [4-6]. On the other hand, hydrogen recycling is similar to the carbonized wall in devices in which the wall temperature is limited at around room temperature [7-9]. Helium glow discharges are widely applied to boronized or carbonized walls and they have been found to be effective for reduction of the hydrogen recycling [16,17]. However these techniques are used without

understanding basic mechanism of the recycling. Dynamic behavior is investigated in JET with a carbon and a beryllium wall [18]. However such data have not been reported for the boron films.

In this study, basic data are obtained for hydrogen implantation, helium ion bombardment, and thermal desorption for boron films. Measurements with high precision are possible by using a liner which has a large surface area as described in chapter 2. Experimental results are presented in chapter 3. In order to understand hydrogen behavior in the boron film, a simple calculation model is proposed and compared to the experimental results, which is discussed in section 4.1. A possible application of the boron films to future devices is discussed in section 4.2.

2. Experimental

An experimental device named SUT (SUrface modification Teststand) is mainly used in this study. Fig. 1 shows a schematic view of the device. The distinctive feature of the device is (1) an ultra high vacuum condition which enables us to prepare clean, impurity free films, (2) an exchangeable liner with a large surface area of 7000 cm^2, which can be heated up to 600 °C, and (3) in-situ Auger electron spectroscopy (AES) measurement.

In this chamber, a cylindrical liner of 400 mm in diameter, 400 mm in height, and 7000 cm^2 in surface area is installed. It is changeable and replaced to new and clean one if necessary. The liner made of stainless steel is mainly used in this study. To investigate the dependence of hydrogen behavior on substrate material, a carbon liner was prepared. The whole liner was made of isotropic graphite IG-430U (made by Toyo Tanso) with the thickness of 5 mm. The dependence on liner material is presented in section 3.6. The liner can be heated up to 600 °C by molybdenum heaters installed in the chamber. The boron film is deposited on the whole inner surface of the liner by a DC glow discharge in B_2H_6 (5%) + He (95%). After the coating, the glow discharges in H_2 and He are carried out. Ions generated in the plasma are accelerated to a few hundreds eV and implanted to the film. The hydrogen absorption and desorption behavior is investigated with pressure change measured by a diaphragm gauge (DG) and a quadrupole mass spectrometer (QMS). Thermal desorption experiments are carried out by raising the whole liner temperature up to 500 °C. All these procedures are done under an ultra high vacuum condition with a background pressure of 10^{-7} Pa, and thus, the impurity concentration in the boron film is kept less than a few percents, which has been confirmed by an in-situ AES.

Fig. 2 shows a diagram of the experimental procedure. It consists of three stages; namely (1) film preparation, (2) discharge experiments, and (3) thermal desorption. In the stage (1), boron films are deposited by the discharge in B_2H_6(5%)+He(95%).

Typical discharge parameters are 2.6 Pa, 0.2A, and 400V. The thickness of the film is monitored by a quartz oscillator. The coating is continued until the thickness on the oscillator reaches 200 nm (typically 72 min.). In most cases, the coating is carried out at around room temperature. The temperature increases during the discharge because of power flow from the plasma, but is kept lower than 70 °C. After the coating, the boron film is once heated up to 500 °C to evacuate H atoms retained originally in the film during the coating.

In the stage (2), hydrogen and/or helium discharges are carried out to investigate hydrogen absorption and desorption characteristics. Typical discharge parameters are 2.6 Pa, 0.2 A, and 400 V for hydrogen, and 2.6 Pa, 0.2 A, and 250 V for helium.

In the stage (3), the liner is heated again up to 500 °C to measure the desorbed number of H atoms from the film, and to reset the boron film into the beginning condition of the stage (2).

After the B-coating and the heating (stage (1)), the stage (2) and the stage (3) were repeated alternately with various schemes of the discharge sequence in the stage (2). The hydrogen discharge, hydrogen discharge + helium discharge, and their repetition are mainly carried out. The procedure in stage (3) is identical through the all series of the experiment.

This procedure allows us to obtain good reproducibility within ±2.5% because the condition of the boron film is once reset by the evacuation of hydrogen atoms with the stage (3). In chapter 3, the experimental results of stage (2) and (3) are mainly presented. Additional coatings are occasionally carried out several times. The boron films which have almost same characteristics can be produced.

Depth profile of H atoms in the film is measured by Elastic Recoil Detection method (ERD) [19]. A substrate of 10 mm × 20 mm made of SS is placed on a sample holder and set at the same condition as the liner surface (see Fig. 1). It is coated together with the liner. After the coating and/or exposure to the plasma, the substrate is taken out and set in another chamber for the ERD. Helium ions of 1.5 MeV are generated by AN-2000 Van de Graaff accelerator and injected to the sample at an incident angle of 10° from the sample surface. A solid state detector for ERD is placed at scattered angle of 20°, with a slit and a myler filter of 6 μm thick to cut the scattered He ions. A detector for Rutherford Back Scattering (RBS) is also set at 150° from the beam to investigate He ion fluence and film thickness [19,20].

Detailed description of the device is given in reference [21].

3. Experimental Results

3.1 Hydrogen glow discharge

Fig. 3 shows a typical time evolution of the total pressure measured by a diaphragm gauge during a glow discharge in hydrogen after the H evacuation by the heating. No change was seen in any gas species other than hydrogen with the QMS measurements. Thus, the total pressure is regarded as the hydrogen pressure. The flow rate and the pumping speed were kept constant at 26 ccm and 15.4 l/s, respectively. Before the ignition of the discharge, the pressure was constant at 2.6 Pa. The pressure decreased with a time constant of 8 sec just after the ignition. It corresponds to pumping characteristic time of this device. The maximum absorption flux is of the same order as the ion flux. This sharp pressure decrease is due to hydrogen absorption into the H depleted top surface of the boron film. The pressure slowly increased when the discharge was continued. It means that the net hydrogen absorption rate decreased due to increase in hydrogen re-emission from the film.

When the discharge was turned off, the pressure once increased and then decreased to a constant value as shown in Fig. 4, which shows the total pressure at around turning off of the discharge for the same data as Fig. 3. This transient increase is regarded as a release of over saturated hydrogen atoms during the discharge. Similar behavior has been reported in tokamaks and Heliotron E [17,22], but it is found for the first time for boron films in a glow discharge condition.

The constant value after the discharge agrees with that before the discharge within ±0.4%, which corresponds to an error bar in Fig. 4. The pressure difference between before and after the termination of the discharge is larger than the error bar. It means that hydrogen atoms are continuously absorbed until the end of the 1 hour discharge. Such a phenomenon has been reported for ion beam injection to some kinds of carbon pieces [23], but found for the first time for a boron film with the plasma irradiation. This slow absorption might be caused by a migration of hydrogen atoms deeper into the film. This effect is discussed in detail in section 3.4 with results of thermal desorption.

Total amount of absorbed H atoms is calculated by integrating pressure drop from the baseline in Fig. 3 multiplied by pumping speed. The value obtained in the case of Fig. 3 is $(9.2\pm0.4)\times10^{16}$ H atoms/cm^2, which is same order as saturation value in other measurements [24-28].

3.2 Helium glow discharge

To investigate the effect of hydrogen desorption by helium ion bombardment, a glow discharge in helium was carried out after the hydrogen discharge of 1 hour. Fig. 5 shows time evolution of the hydrogen pressure measured by QMS. The QMS signal is converted to absolute partial pressure by a calibration with the diaphragm gauge. The pressure rapidly increased with the same time constant as the pumping system. It means that hydrogen atoms are immediately desorbed by the He ion impact. The pressure decreased during the discharge and became lower than the detection level within 15 min. Total amount of desorbed hydrogen atoms is calculated by the similar procedure as in the case of hydrogen discharge, and estimated to be $(1.3\pm0.4)\times10^{16}$ H atoms/cm^2. It corresponds to 15% of the absorbed hydrogen during 1 hour H_2 discharge.

To investigate a recovery of hydrogen absorption capability by the helium glow discharge, a hydrogen discharge was carried out after the helium glow discharge as schematically shown in upper part of Fig. 6. The rapid and strong absorption was observed again in the initial phase of the discharge. It corresponds to reduction of H recycling with He glow discharge in fusion experimental devices. The absolute value of the pressure change is indicated in the figure to compare absorbed and desorbed number clearly. Total number of absorbed H during the second H_2 discharge is larger than the one desorbed during the He discharge. This indicates that hydrogen atoms are accumulated on the surface by repeating H_2 and He discharges alternately. This effect is another new finding of this study, and discussed again in section 3.4 with the results of thermal desorption experiments.

The behavior is understood qualitatively as follows :

Hydrogen atoms retained in the near surface region are detrapped by He ion bombardment. Some of the detrapped H atoms are recombined and desorbed from the surface as H_2. Some migrate deeper into the film and retrapped. The hydrogen atoms in near surface region are evacuated in this manner. Thus, strong and short time absorption occurs during the initial phase of the second H_2 discharge which follows the He discharge and the absorbed number is larger than the desorbed one.

3.3 Thermal desorption

To investigate thermal desorption characteristics, the whole liner was heated up to 500 °C. Fig. 7 shows time evolution of H_2 pressure measured by QMS and the liner temperature, during the heating after the 1 hour H_2 discharge.

The liner temperature was increased linearly with a rate around 10 °C/min. The H_2 pressure increased almost linearly until a peak value around 400 °C. The pressure

decreased when liner temperature was increased to and kept at 500 °C for 30 minutes. The same result is plotted in Fig. 8 against the liner temperature. The peak position at 380 °C is seen more clearly. Similar behavior has been reported in refs. [29,30] for small test species. It is demonstrated for relatively large surface area of 7000 cm^2.

Total number of desorbed H atoms is calculated by integrating the curve in Fig. 7 and estimated to be $(11\pm0.05)\times10^{16}$ H atoms/cm^2. This is slightly larger than but close to the number of absorbed H atoms during the H_2 discharge (see section 3.1).

The accuracy is higher in the thermal desorption measurement (±0.5%) than in the H_2 discharge (±4%) or the He discharge (±30%) mainly because the drift of the baseline is small compared to the signal intensity in the thermal desorption. Detailed discussion about the accuracy is given in a reference [21].

3.4 Discharge experiments and thermal desorption

As mentioned in chapter 2, a series of discharge experiments (stage 2) and the thermal desorption experiment (stage 3) are repeated with changing the discharge procedure in the stage 2 . In this section, net absorbed number of H atoms during the stage 2 and desorbed one during the stage 3 are compared.

To confirm slow and continuous absorption of H atoms after the near saturation at 30 minutes, a hydrogen discharge of 3 hours was carried out. The results are shown in Fig. 9, where vertical axis shows retained number of H atoms estimated by integration of the pressure change. The number increased continuously up to 3 hours and became 1.3 times higher than that at 1 hour. Even when the discharge continued up to 10 hours, the absorption continued without saturation.

The dotted lines in the figure show time evolution of retained H during thermal desorption experiments after 1 hour and 3 hours H_2 discharge, respectively. The retained number decreased and returned to the initial value in each case. It means that most of absorbed H atoms can be desorbed by the heating. In every thermal desorption, the desorbed number was slightly larger than the absorbed one in the preceded hydrogen discharges. It is probably due to H atoms deposited during the coating and remained after the heating.

To confirm H accumulation effect by H_2/He discharges, glow discharge in H_2 and He (each 15 min.) were repeated 4 times after the H_2 discharge of 1 hour. Similar to Fig. 9, the retained number of H atoms is shown in Fig. 10. The number of H atoms decreased during He discharges by the ion impact desorption. The number increased rapidly at initial phase of H_2 discharge after the He discharge. It corresponds to hydrogen trapping in evacuated near surface region as mentioned in section 3.2. After the rapid absorption, the hydrogen absorption continued slowly without saturation until

the end of the discharge. The retained number increased gradually by the repetition of the discharges.

It should be noted that the shape of the curves are almost same during the repetition. It means that hydrogen absorption and desorption behaviors at initial phase of the discharges are governed by hydrogen atoms of near surface region and not affected by the slow accumulation of the hydrogen atoms deeper into the film. The results of thermal desorption experiments are also shown in the figure, which shows that most of the accumulated H atoms can be desorbed by the heating in this case, too.

From these results and the shape of the curve in Fig. 7, which has the peak value, we can conclude that hydrogen atoms implanted during the discharges can be evacuated by the heating up to 500 °C. The required temperature for the H evacuation is regarded as 400 °C from the peak position. This temperature is much lower than that for carbon wall of 900 °C [31] and B/C coating of 700 °C [4,32]. This is important for application to a fusion device and discussed later in section 4.2.

This fact means that the number of retained H atoms can be measured by the thermal desorption experiments. As mentioned in section 3.3, the measurements with high accuracy are possible.

To investigate slow desorption effect during the long time He discharge, 1 hour He discharge was carried out. The desorbed number is plotted in Fig. 11 for the thermal desorption experiments after (a) a 1 hour H_2 discharge, (b) 1 hour H_2 discharge + 15 minutes He discharge, and (c) 1 hour H_2 discharge + 1 hour He discharge. The retained number decreased by applying He discharge for a longer time up to 1 hour. It means that the desorption of H atoms continues up to 1 hour in the He discharge though the hydrogen partial pressure becomes lower than the detection level in QMS within 15 minutes as mentioned in section 3.2.

To show the slow absorption effect more quantitatively, desorbed number is plotted in Fig. 12 for the thermal desorptions after (a) 3 hour H_2, (b) 1 hour H_2 + He/H_2 for total 8 times (15 min. each), and (c) H_2/He total 5 times (1 hour each).

The series (a) and (b) correspond to Fig. 9 and Fig. 10 respectively. It was difficult to directly compare the accumulation rate in Fig. 9 and Fig. 10 only from the pressure analysis during the discharge. It is shown from the thermal desorption experiments that the rate in continuous hydrogen discharge is 10% higher than the increasing rate of the envelope in H_2/He discharge. It should be noted that the ion impact detrapping cross-section cannot be compared only from these results because the phenomena are complex. The difference is discussed in chapter 5.

The total length of the hydrogen discharge is same between the series (a) and (c). However, the retained number is clearly larger in the series (c) even though hydrogen atoms are desorbed during the He glow discharges. Thus it is concluded that the He ion bombardment has a certain impact to accumulate hydrogen atoms in boron films.

3.5 Depth profile measurements

The depth profile of the H atoms was investigated by using the ERD method. Fig. 13 shows depth profile obtained in cases of (a) after the B-coating and the thermal desorption, (b) 1 hour exposure to the H_2 glow, and (c) 3 hours exposure.

The density was low and constant as a function of the depth after thermal desorption (case a). The hydrogen was retained up to 110 nm, which was same as the film thickness measured by RBS method. It means that hydrogen atoms were retained only in the boron film and not penetrated to the stainless steel substrate. The thickness was roughly half of that measured by quartz oscillator thickness monitor. It is probably because the location of the thickness monitor is slightly inside the liner. The density was about 1/8 of that of the sample just after the coating before the heating. Those H atoms are retained during the deposition of the film and difficult to remove by the heating lower than 500 °C probably due to larger bonding energy than others. It is consistent with the fact that the desorbed number during the thermal desorption experiments is slightly larger than the absorbed one.

In cases of (b) and (c), the density of only near surface region (~70nm) increased. When the discharge continued for 3 hours, the peak density increased and the peak position slightly shifted to deeper level compared to the case of the 1 hour exposure.

The resolution of the ERD measurements is around 15 nm [34]. The real profile of hydrogen is sharper if the resolution is taken into account. Relation between detected depth profile $N_{DET}(x)$ and real profile $N_{REAL}(x)$ is described as follows with an assumption of gaussian distribution,

$$N_{DET}(x) = \int N_{REAL}(t-x) \bullet g(t)dt$$

where

$$g(t) = \frac{1}{\sigma\sqrt{\pi}} \exp\left(-\frac{t^2}{\sigma^2}\right)$$: Gaussian distribution function

σ : resolution

x : depth

For simplicity, we assumed real density profiles of square type with non-zero background level as indicated hatched area in Fig 14. The background level was determined from the case (a) in Fig. 13 since it is uniform. The standard profile (A) and resolution σ were determined to obtain best fit to the profile of 1 hour (case (b) in Fig. 13). The saturation level was estimated to be 1.0×10^{22} atoms/cm^3, which is same order as the density of boron atoms. It should be noted that the concentration of the

background level is much lower than the saturation level in the real profile, though they seem comparable in detected profile in Fig. 12.

We gave two kinds of square type distribution to $N_{REAL}(x)$for the case of 3 hours exposure; (B) density increase (open squares) and (C) depth increase (closed squares). A rate of the increase was taken as 30% from the increasing rate of retained H shown in thermal desorption experiments. The calculated profiles are indicated in Fig. 14. In spite of small difference between (B) and (C), the peak clearly shifted to the deeper side in (C) compared to (B) and (A). In addition the assumption (C) seems more reasonable if we assume the saturation density.

Thus, it is concluded that hydrogen atoms are retained only in near surface region of ~10 nm, which is same order as its implantation range and much smaller than the film thickness of 110 nm. When the film is exposed to an H_2 discharge for a longer time, increase in H retention can be explained by the hydrogen migration deeper into the film, but the migration is limited in the surface region. These findings are important for application and discussed again in section 4.2.

3.6 Dependence on substrate materials

Fig. 15 shows a time evolution of the hydrogen pressure during the H_2 discharge with boron films on stainless steel (SS) and isotropic graphite (C). The strong absorption at initial phase and the long continuing absorption were also observed with C liner. The effect of helium discharge with C liner was similar to that with SS liner. Fig. 16 shows the results of thermal desorption experiments after 1 hour H_2 discharges. The shape of the curve is similar in both cases. It is concluded that the hydrogen behavior in boron film is not affected by the substrate material except for the absolute value. The difference might be attributed to difference in effective surface area due to difference in surface morphology.

4. Discussion

4.1 Modeling of hydrogen behavior

Several models to describe hydrogen behavior in graphite and amorphous carbon have been reported [31,33-36]. Most of the models assume the existence of trapped and solute (mobile) hydrogen atoms, and the effects of de-trapping, trapping, diffusion, and desorption are considered. The trapping state of H atoms in boron film is not well understood. However, it is confirmed experimentally that the hydrogen atoms do not move at least for a few days at around room temperature. It means that hydrogen atoms are trapped in the boron film similar to the H atoms in carbon. Thus a simple model is

developed based on the conventional models for graphite and amorphous carbon, and the calculated results are shown in this section.

First, the transient release of the H atoms after the termination of the H_2 discharge is modeled. It is reported in JET that the hydrogen release after the discharge is attributed to the thermal detrapping of the trapped H atoms followed by the release as H_2 through the recombination [18]. However, hydrogen atoms do not move in this experimental condition as mentioned above. We assume that most of the hydrogen atoms are trapped after the termination of the discharge except for over saturated H atoms due to H implantation from the discharge. The hydrogen release is attributed to recombination of the over-saturated H atoms. Then the differential equation is written as follows;

$$\frac{\partial c_s}{\partial t} = -2k_{ss}c_s^2 - k_{ss}^{'}c_s c_t \qquad (1),$$

where c_S and c_t are the hydrogen density of "solute" and "trapped" respectively. Two kinds of recombination process, namely "solute - solute" and "trapped - solute", are possible. They correspond to first and second term of the right hand side of equation (1), respectively. Time evolution of H re-emission is calculated based on the equations (1) for two extreme cases, that is, the recombination occurs only through the process of (i) "solute - solute" or (ii) "trapped - solute". Both can be solved analytically and the results are

$$\Phi = \frac{R_i}{2k_{ss}} \frac{1}{\left(t + 1/2k_{ss}c_0\right)^2} \qquad (2)$$

for assumption (i) and

$$\Phi^{'} = c_0 R_i \cdot k_{ss}^{'} c_t \exp\left(-k_{ss}^{'} c_t t\right) \qquad (3)$$

for assumption (ii), where R_i is implantation range and c_0 is initial concentration of over saturated H atoms. The $c_0 R_i$ corresponds to total amount of over saturated H atoms and estimated to be 1×10^{15} H atoms/cm^2 by integrating the curve in Fig. 4.

The results are shown in Fig. 17(a) and (b) for the assumption (i) and (ii), respectively. The experimental data for Φ_{wall} are calculated from the pressure change by using the mass balance equation,

$$V\frac{dp}{dt} = Q - S_p p + \beta A \cdot \Phi_{wall} \qquad (4),$$

where V is volume of the chamber, Q source rate due to external gas injection, p pressure, Sp pumping speed, A surface area of the liner, and β a conversion factor. The solid line in the figure shows results of the calculation. In Fig. 17(a), the calculated results agree well with the experimental results. On the other hand, the calculation does not give agreement with the experimental results in Fig. 17(b). It is concluded that the recombination of two solute H atoms is dominant. The product of

k_{SS} R_i is estimated from the best fitting value. The R_i is estimated to be 6.5 nm based on TRIM code calculation [37], and then, the k_{SS} is estimated as 7.8×10^{-24} cm^3/s.

Based on the findings about the recombination, the transient behavior just after turning on and off of the discharge is investigated. Here, the slow migration of the H atoms can be neglected. In addition, following conditions are assumed; (a) thermal detrapping can be neglected at around room temperature, (b) ion implantation is uniform in depth within its implantation range, and (c) ion impact detrapping is also uniform.

The differential equation can be written as follows;

$$\frac{\partial c_s}{\partial t} = S_r - 2k_{ss}c_s^2 - k_{st}c_s(c_T - c_t) + \sigma_d \Phi_i c_t \quad (5),$$

$$\frac{\partial c_t}{\partial t} = k_{st}c_s(c_T - c_t) - \sigma_d \Phi_i c_t \quad (6),$$

where c_T is the density of the trap site, k_{ST} trapping rate coefficient, and σ_d the ion impact de-trapping cross-section. The S_r denotes source term due to hydrogen implantation. The S_r is estimated from the experimental value of the maximum absorption flux assuming that all of the injected hydrogen atoms are absorbed at initial phase. The ion flux Φ_i is estimated from the discharge current. The maximum absorption flux is 2 times higher than Φ_i. The atomic hydrogen which is generated in the plasma might contribute to the hydrogen absorption.

In quasi steady state ($\partial/\partial t \approx 0$), the equations (5) and (6) reduce to

$$S_r = 2k_{ss}c_s^2 \quad (7),$$

$$k_{st}c_s(c_T - c_t) = \sigma_d \Phi_i c_t \quad (8).$$

From the equation (7), c_S is estimated to be 8.8×10^{21} H atoms/cm^3. If we assume the saturation density of 4×10^{22} H atoms/cm^3, which corresponds to H/B ratio of 0.4, the ratio

$$k_{ST}/\sigma_d = 0.21 \text{ [cm/s]} \quad (9)$$

is obtained from the equation (8). It means that a larger trapping probability corresponds to a larger detrapping probability. The estimated concentration of the solute hydrogen corresponds to 20% of the saturation density. It should be noted that the following results do not strongly depend on the trap density.

The time evolution of the hydrogen desorption flux after the termination of the H_2 discharge is calculated for wide range of trapping and de-trapping probability. The results are shown in Fig. 18. When the detrapping cross-section is smaller as $\sigma_d \sim 10^{-22}$ cm^2, the strong desorption is observed which is higher than the experimental results by an order as a curve (b). The strong desorption rapidly decreased within a second when the trapping and detrapping probability are sufficiently large as a curve (a). The hydrogen atoms in solute state under the ion bombardment are immediately trapped and the over saturated H atoms are released with a time constant of ~1 min, which shows similar behavior with the exprtimental results. In this experimental condition, the rapid

desorption could not be observed because the time constant of the desorption is much smaller than that of pumping system of 8 sec. Thus it is concluded that the calculated results agree with the experimental result with larger trapping and detrapping rate. The value $\sigma_d \sim 10^{-22}$ cm^2 corresponds to the condition in which the time constant for the trapping is comparable to that for the desorption.

Fig. 19 shows the hydrogen desorption behavior just after the ignition of the helium glow discharge. Here, the trapping and detrapping probabilities are assumed to be same and the results are indicated for three cases; namely, trapping (and thus the de-trapping) probability is (a) large enough, (b) small enough, and (c) intermediate, compared to the desorption probability. In cases (b) and (c), the sharp desorption after the ignition is not observed. The time behavior is similar to the experimental results in case (a), except for the difference in absolute value. The difference can be attributed to the difference in ion induced detrapping cross-section. It results in the change in the ratio of k_{st}/σ_d because trapping probability may be same as that during the hydrogen discharge. Fig. 20 shows the best fitting of the calculated data together with the experimental results. It is found that if we assume the detrapping cross-section of 5 times lower than that for hydrogen ion impact, the experimental results can be well reproduced.

From these considerations, it is found that hydrogen desorption during the He discharge and hydrogen release after the termination of the hydrogen discharge can be described by the model if we assume that the hydrogen trapping and detrapping rates are large enough compared to the desorption rate through the recombination. The hydrogen atoms of around 20% are considered to be in solute state with repeating trapping and detrapping under ion bombardment. The slow absorption effects may be driven by the migration of these solute atoms.

The time evolution of the absorption flux at initial phase of the H_2 discharge is calculated for the case of larger trapping and detrapping probabilities. Fig. 21 shows calculated results together with the experimental results (solid thick line). In contrast to the results in Figs. 18 and 19, calculated result does not agree with the experimental results. The rapid decrease of absorption flux, which is observed in the experimental result is not reproduced, because the implanted hydrogen atoms could be trapped and not re-emitted in calculated results. A possible explanation for this difference is that the atomic hydrogens, which are not implanted into the film, accumulate on the surface and re-emitted from the initial phase. To understand this behavior quantitatively, the depth profile of hydrogen implantation must be considered.

4.2 Application for protection wall against tritium permeation

Through this study, it is demonstrated that (1) hydrogen atoms are retained only in near surface region around their implantation range, and (2) most of the implanted hydrogen atoms can be desorbed by the heating up to 400 °C. These favorable characteristics gives an idea of a protection wall against tritium permeation [19].

In future fusion devices, the first wall is exposed to charge exchange neutral tritium atoms, which have relatively high energy. It will induce considerable tritium inventory and its permeation to cooling channels. However if the wall is coated by a boron film, implanted tritium atoms are retained only in near surface and desorbed from the film toward the plasma side. It is possible to keep the temperature of the first wall high by utilizing heat load from the plasma. In this case, the first wall design becomes easier with boron coating because the required temperature for the tritium evacuation is much lower than that for carbon wall, and thus, the temperature difference between the first wall and the coolant becomes smaller.

The present experiment has shown up these very promising characteristics of boron films. It is necessary to study this possibility further by additional experiments such as an actual investigation on permeation etc.

5. Conclusion

It is found that there are two components in hydrogen absorption into the boron film at around room temperature. One is strong and short absorption to H depleted near surface. The other is the slow and long lasting absorption. The slow absorption are considered to be caused by the hydrogen migration deeper into the film following to the ion impact detrapping.

Similarly, the helium ion impact causes not only H desorption but also migration of detrapped hydrogen atoms deeper into the film, and thus, the hydrogen atoms are accumulated in the film when the H_2 and He discharges are repeated alternately. The depth profile measured by ERD gives consistent results with this consideration.

The hydrogen atoms are retained only in the near surface region which is same order as its implantation range and much smaller than the film thickness of 110 nm. Most of them can be released by the heating up to 400 °C, even when the boron film is exposed to the hydrogen discharge for a long time. These are favorable characteristics for applying B-films as a protection wall against tritium permeation.

A simple model to describe hydrogen behavior is given. It is found that the recombination of two solute hydrogen atoms are dominant in the desorption process, and the recombination coefficient is estimated to be 7.8×10^{-24} cm^3/s from the analysis for transient hydrogen release just after the termination of the hydrogen discharge.

Transient behavior after the ignition of H_2 and He discharge is modeled based on the findings about the recombination. The calculated results with this model agree fairly well with the experimental results. It is found through the calculation that the hydrogen atoms of around 20% of the saturation density are in solute state, which is maintained with a balance between trapping and detrapping.

REFERENCES

[1] J. Winter, J. Nucl. Mater. 145-147 (1987) 131.

[2] J. P. Coad, K. H. Behringer and K. J. Dietz, J. Nucl. Mater. 145-147 (1987) 747.

[3] N. Noda et al., Jpn. J. Appl. Phys. 25 (1986) L397.

[4] J. Winter et al., J. Nucl. Mater. 162-164 (1989) 713.

[5] G. L. Jackson et al., J. Nucl. Mater. 196-198 (1992) 236.

[6] M. Saidoh et al., Fusion Engineering and Design 22 (1993) 271.

[7] U. Schneider et al., J. Nucl. Mater. 176&177 (1990) 350.

[8] H. F. Dylla et al., J. Nucl. Mater. 176&177 (1990) 337.

[9] H. Yamada et al., Jpn. J. Appl. Phys. 33 (1994) L1638.

[10] P. R. Thomas, J. Nucl. Mater. 176&177 (1990) 3.

[11] J.D. Strachan et al., J. Nucl. Mater. 217 (1994) 145.

[12] N. Noda, J. Nucl. Mater. 220-222 (1995) 623.

[13] J. Ehrenberg, J. Nucl. Mater. 162-164 (1989) 63.

[14] S. Higashijima et al., J. Nucl. Mater. 220-222 (1995) 375.

[15] N. Noda, In Contribution to high-temperature plasma physics, Akademie Verlarg, Berlin (1994) 21.

[16] D. S. Walsh, B. L. Doyle, W. R. Wampler and A. K. Hays, J. Vac. Sci. Technol. A9 (1991) 727.

[17] N. Noda et al., J. Nucl. Mater. 162-164 (1989) 769.

[18] J. Ehrenberg et al., J. Nucl. Mater. 196-198 (1992) 992.

[19] K. Tsuzuki et al., J. Nucl. Matel. In press

[20] M. Natsir et al, Vacuum 47 (1996) in press.

[21] A. Sagara et al., to be publiched in Rev. Sci. Instrum.

[22] P. Andrew and M. Pick, J. Nucl. Mater. 220-222 (1995) 601.

[23] A. A.Haasz and J. W. Davis, J. Nucl. Mater. 209 (1994) 155.

[24] M. Yamage, T. Ejima, H. toyoda and H. Sugai, J. Nucl. Mater. 196-198 (1992) 618.

[25] B. L. Doyle, W. R. Wampler, D. K. Brice and S. T. Picraux, J. Nucl. Mater. 93&94 (1980) 551.

[26] Y. Yamauchi et al., J. Nucl. Mater. 220-222 (1995) 851.

[27] J. Von Seggern et al, J. Nucl. Mater. 176&177 (1990) 357.
[28] D. S. Walsh et al., J. Vac. Sci. Technol. A 9 (1991) 727.
[29] H. Toyoda, T. Isozumi, H. Sugai and T. Okuda, J. Nucl. Mater. 162-164 (1989) 732.
[30] T. Hino et.al, Thin solid films, 253 (1944) 518.
[31] W. Moller, J. Nucl. Mater. 162-164 (1989) 138.
[32] R. Jimbou, M. Saido, N. Ogiwara, and T. Ando, J. Nucl. Mater. 196-198 (1992) 958.
[33] K. Morita, K. Ohtsuka and Y. Hasebe, J. Nucl. Mater. 162-164 (1989) 990.
[34] B. L. Doyle, W. R. Wampler, D. K. Brice and S. T. Picraux, J. Nucl. Mater. 93&94 (1980) 551.
[35] S. Yoshida, H. Sugai and H. Toyoda, Jpn. J. Appl. Phys. 28 (1988) 1101.
[36] A. A. Haasz, P. Franzen, J. W. Davis, S. Chiu and C. S. Pitcher, J. Appl. Phys. 77 (1995) 66.
[37] J.P.Biersack and W.Eckstein, Appl. Phys. A34 (1984) 73-94.

Figure Captions

Fig. 1 Cross-sectional view of main chamber of SUT.

Fig. 2 Schematic diagram of experimental procedure. The procedure consists of three stages; (1) film preparation, (2) discharge experiments, and (3) thermal desorption.

Fig. 3 Time evolution of total pressure during glow discharge in hydrogen. The discharge current and voltage are 0.2 A and 400 V, respectively. The pumping speed (15.4l/s) and hydrogen flow rate (26.0 ccm) are kept constant. The pressure decreased due to hydrogen absorption into the boron film.

Fig. 4 Total pressure around turning off of the discharge for same data as Fig. 3. The pressure once increased and then decreased to the constant value, which is larger than the pressure during the discharge.

Fig. 5 Time evolution of hydrogen partial pressure measured by QMS. The discharge current and voltage are 0.2 A and 500 V, respectively.

Fig. 6 Absolute value of pressure change during H_2/He discharges. The procedure is schematically shown in upper part of this figure.

Fig. 7 Time evolution of hydrogen pressure and liner temperature during thermal desorption.

Fig. 8 Hydrogen pressure against liner temperature for same data as Fig. 7.

Fig. 9 Hydrogen accumulation during long time H_2 discharge. Dotted lines show decrease of hydrogen atoms during thermal desorption.

Fig. 10 Time evolution of retained number of H atoms when H_2 and He discharges are repeated alternately. The data during thermal desorption are also shown.

Fig. 11 Number of hydrogen atoms desorbed by heating. The decreased number corresponds to desorbed number of H atoms during the He discharge.

Fig. 12 Comparison of desorbed number of H atoms during thermal desorption experiments after (a) 3 hours H_2 discharge (case in Fig. 9), (b) 1 hour H_2 and repetition of He/H_2 for 4 times (case in Fig. 10), and (c) 1 hour H_2 and repetition of He/H_2 for 2 times (1 hour each, total 5 hours, H_2 total 3 hours).

Fig. 13 Depth profile of H atoms measured by ERD

Fig. 14 Calculation of detected profile from real profile. Real profile of square type is assumed. The experimental results are reproduced .

Fig. 15 Time evolution of hydrogen pressure during H_2 discharge with boron film on stainless steel and graphite.

Fig. 16 Time evolution of hydrogen pressure during heating with boron film on stainless steel and graphite.

Fig. 17 Hydrogen desorption after termination of hydrogen discharge. The open circles show experimental results. The lines show calculated results for two extreme cases ;(a) recombination of two solute H atoms is dominant, (b) recombination of solute and trapped H atoms is dominant. The assumption (a) agrees better with the experimental results.

Fig. 18 Time evolution of hydrogen pressure after termination of discharge. When the smaller trapping and detrapping probability are used (b) large desorption flux could be observed.

Fig. 19 Hydrogen desorption at initial phase of He discharge. Calculated results are shown for three cases; trapping and detrapping probability is (a) large enough, (b) intermediate, and (c) small enough.

Fig. 20 Hydrogen desorption during He discharge. The calculated results agree well with the experimental results if the ion induced detrapping cross-section of 5 times smaller than that of hydrogen ion impact.

Fig. 21 Hydrogen absorption at initial phase of H_2 discharge. Calculated results are shown for the case of large trapping and detrapping probability.

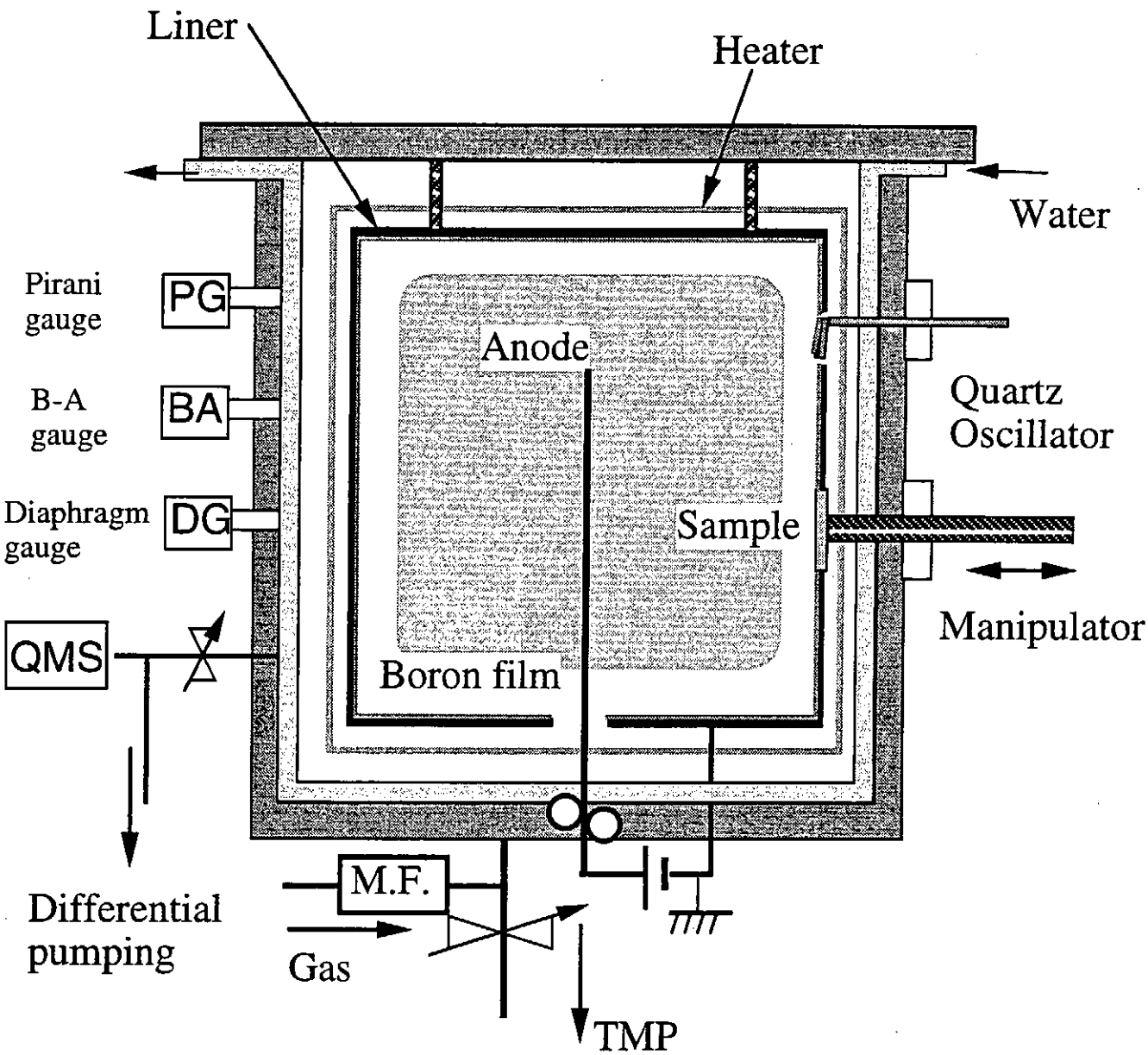

Fig. 1 Cross-sectional view of main chamber of SUT.

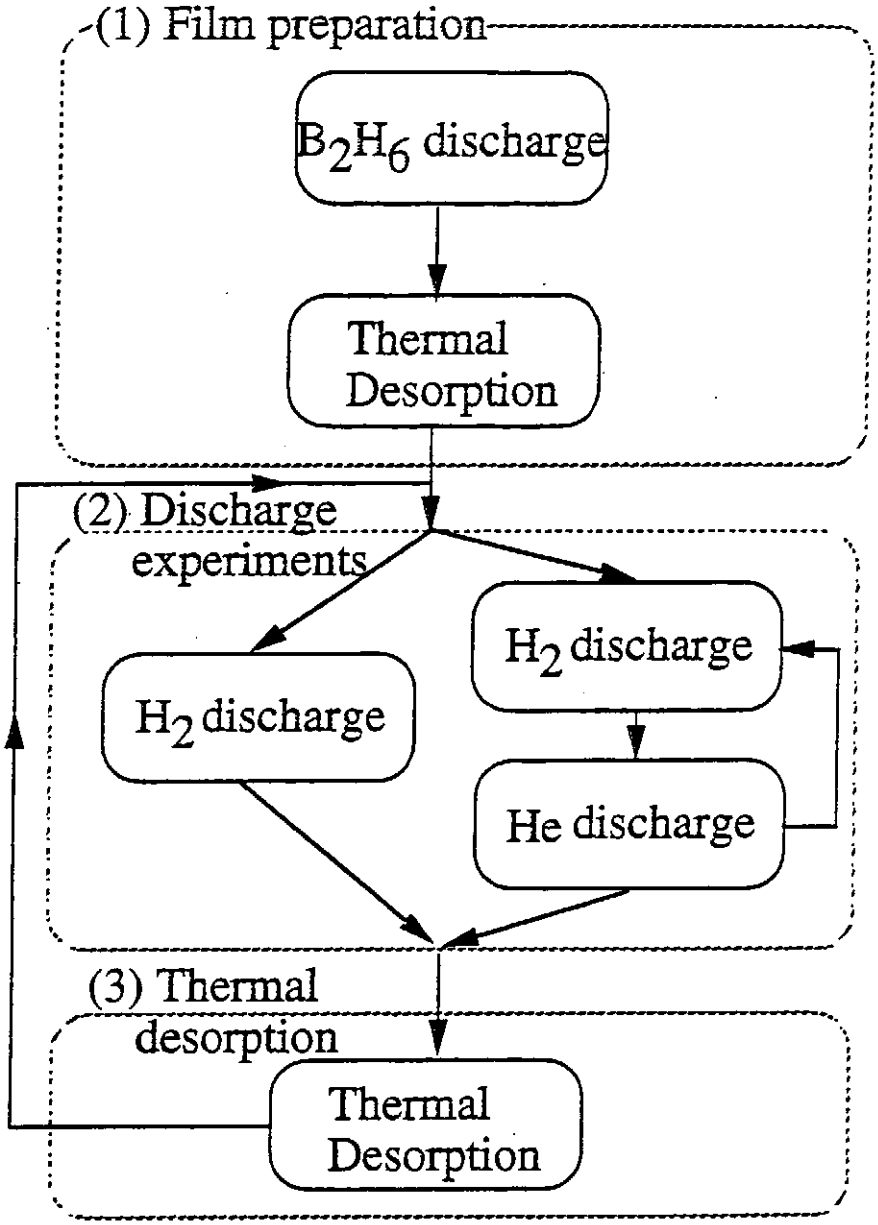

Fig. 2 Schematic diagram of experimental procedure.
The procedure consists of three stages; (1) film preparation, (2) discharge experiments, and (3) thermal desorption.

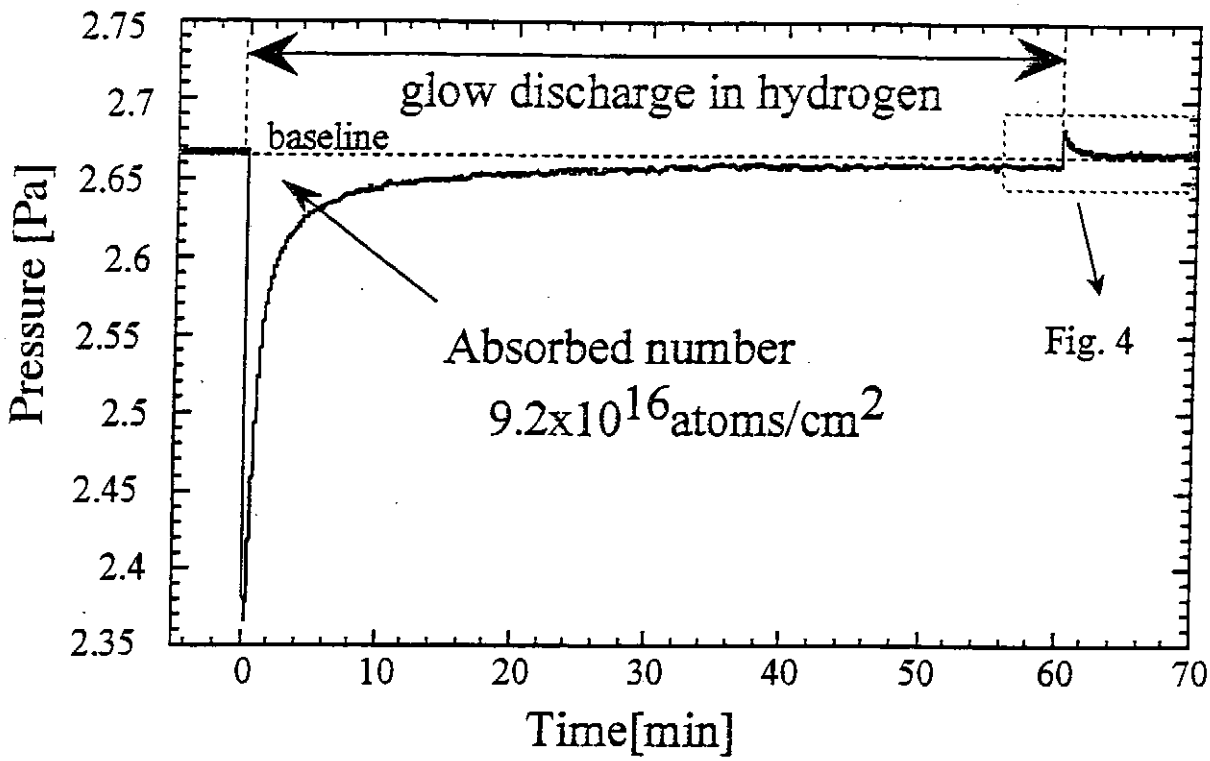

Fig. 3 Time evolution of total pressure during glow discharge in hydrogen. The discharge current and voltage are 0.2 A and 400 V, respectively. The pumping speed (15.4l/s) and hydrogen flow rate (26.0 ccm) are kept constant. The pressure decreased due to hydrogen absorption into the boron film.

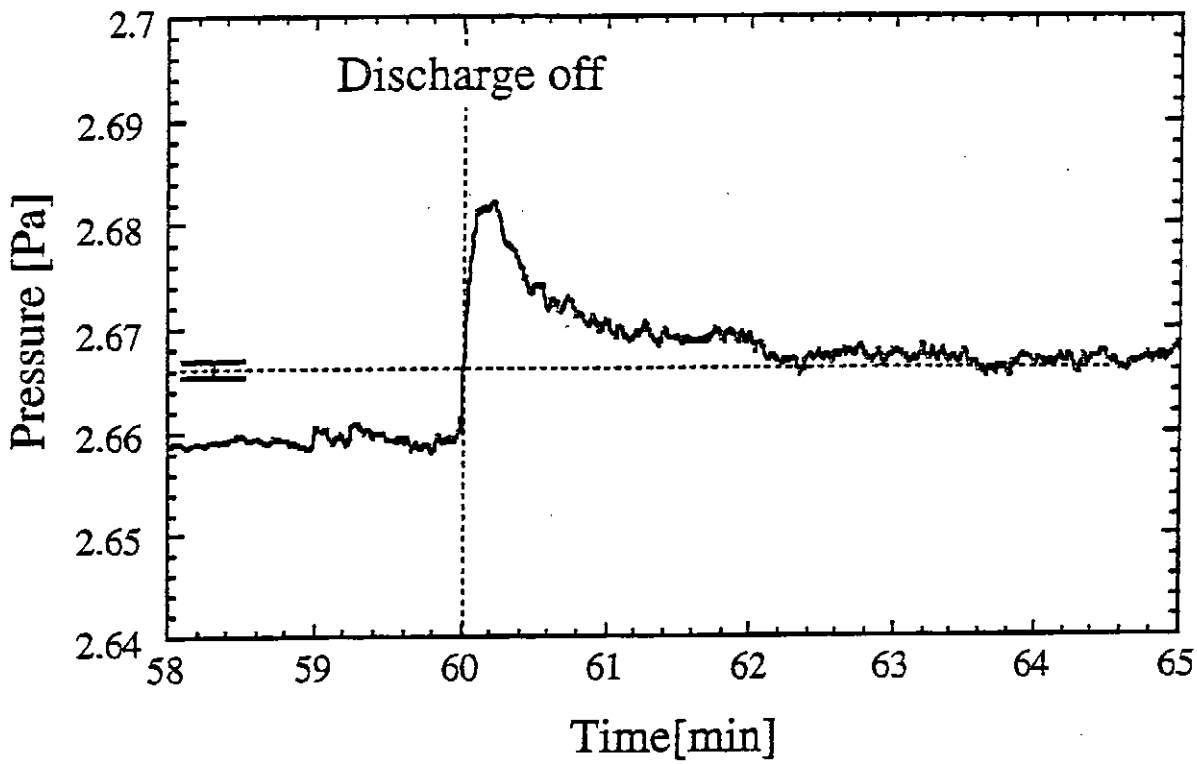

Fig. 4 Total pressure around turning off of the discharge for same data as Fig. 3. The pressure once increased and then decreased to the constant value, which is larger than the pressure during the discharge.

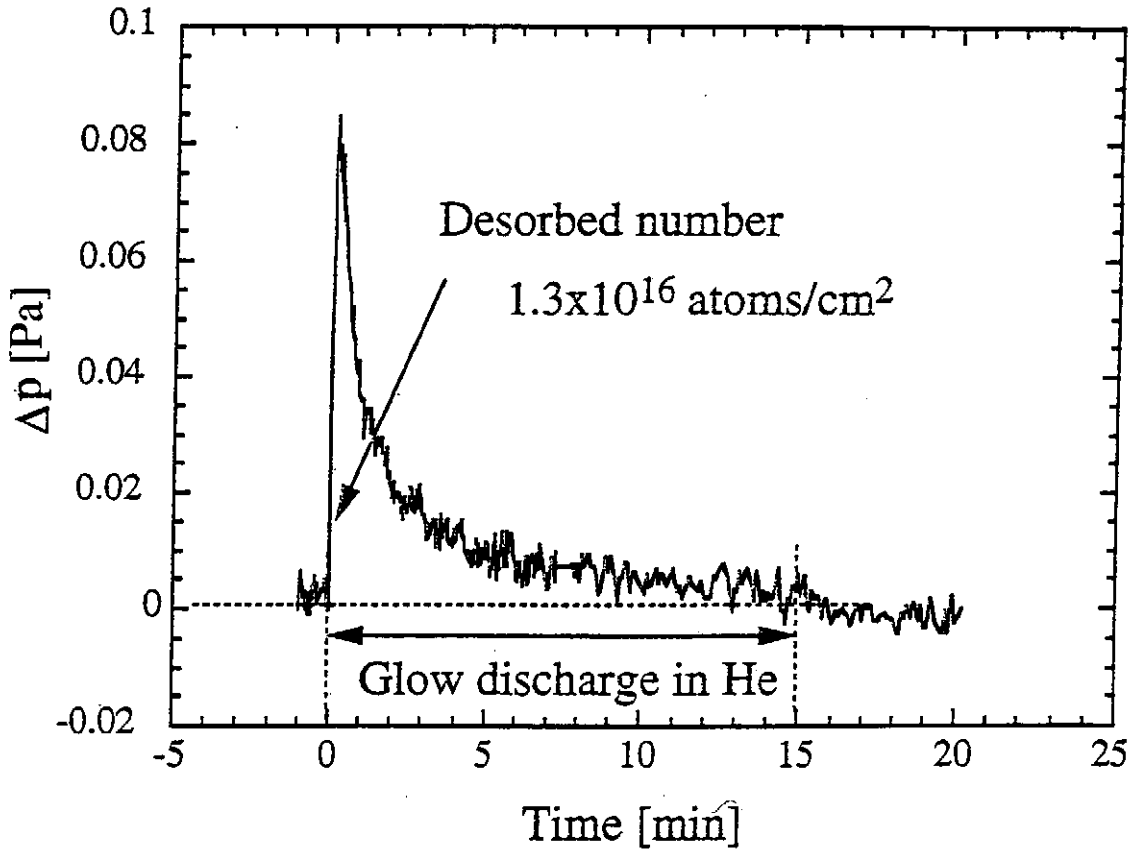

Fig. 5 Time evolution of hydrogen partial pressure measured by QMS. The discharge current and voltage are 0.2 A and 500 V, respectively.

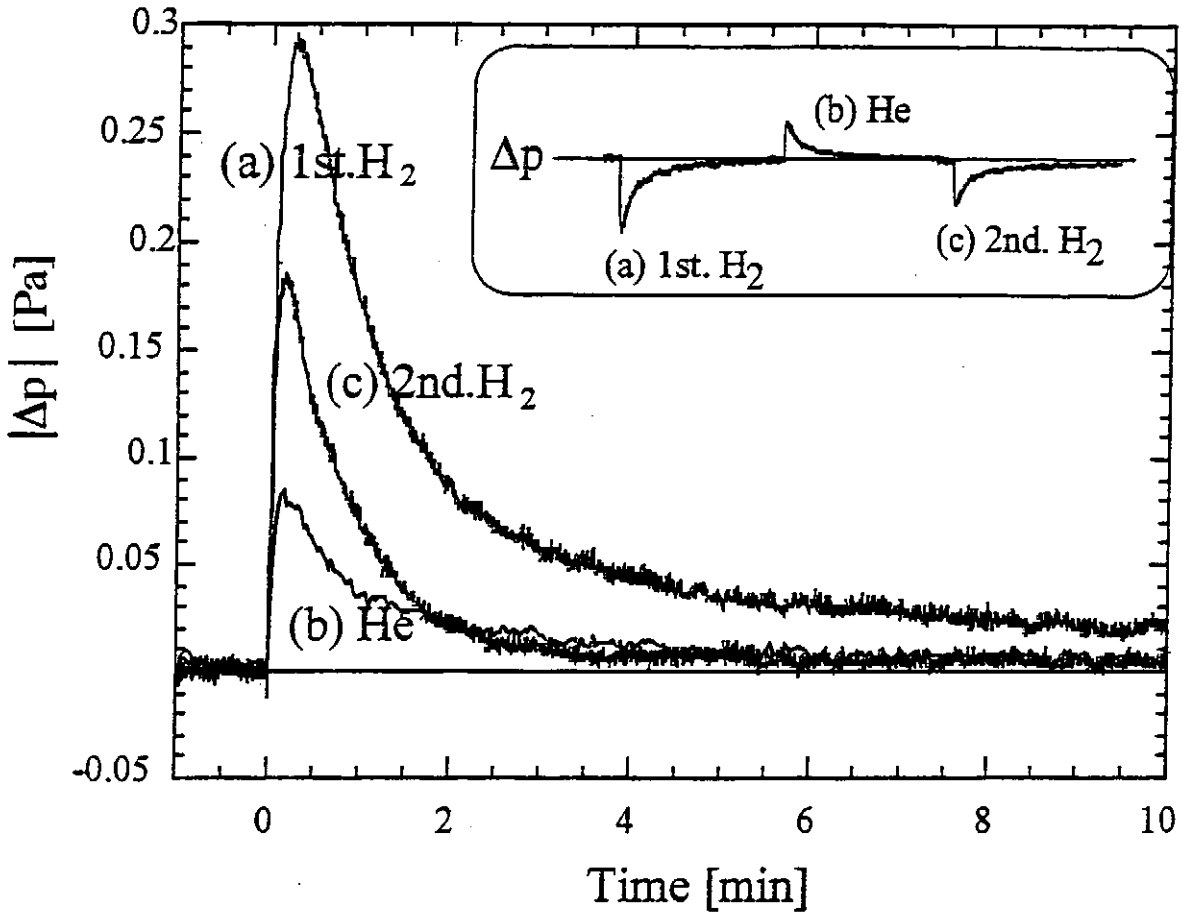

Fig. 6 Absolute value of pressure change during H_2/He discharges. The procedure is schematically shown in upper part of this figure.

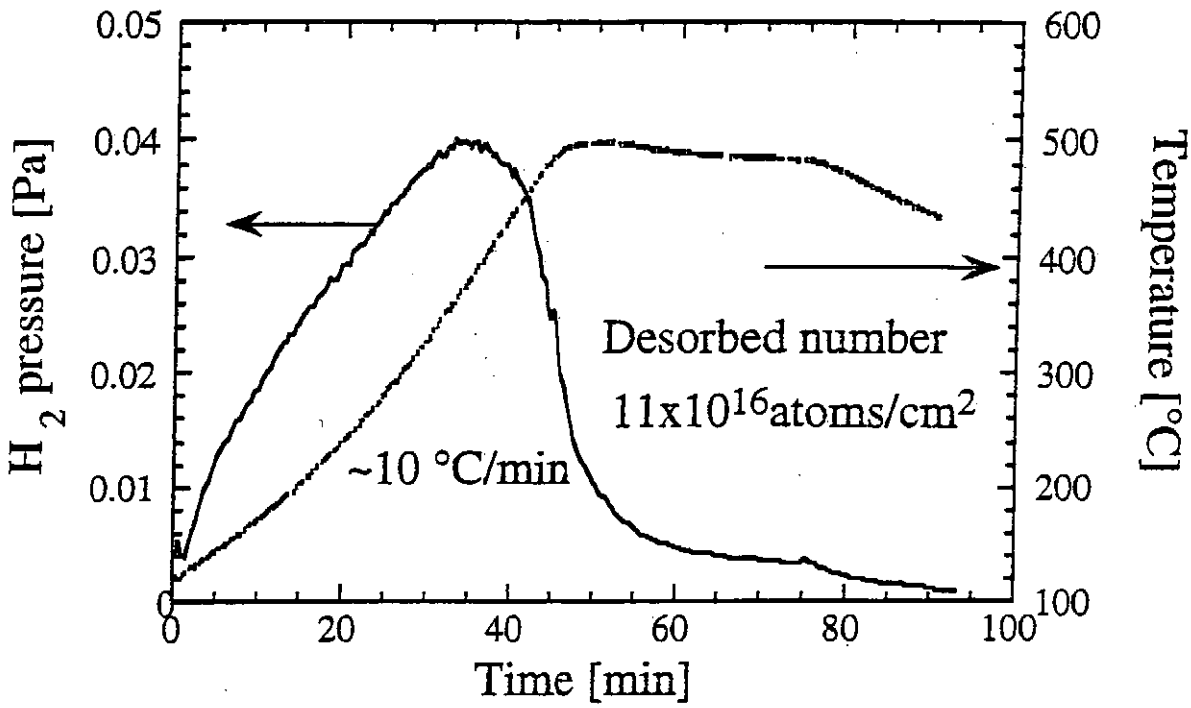

Fig.7 Time evolution of hydrogen pressure and liner temperature during thermal desorption.

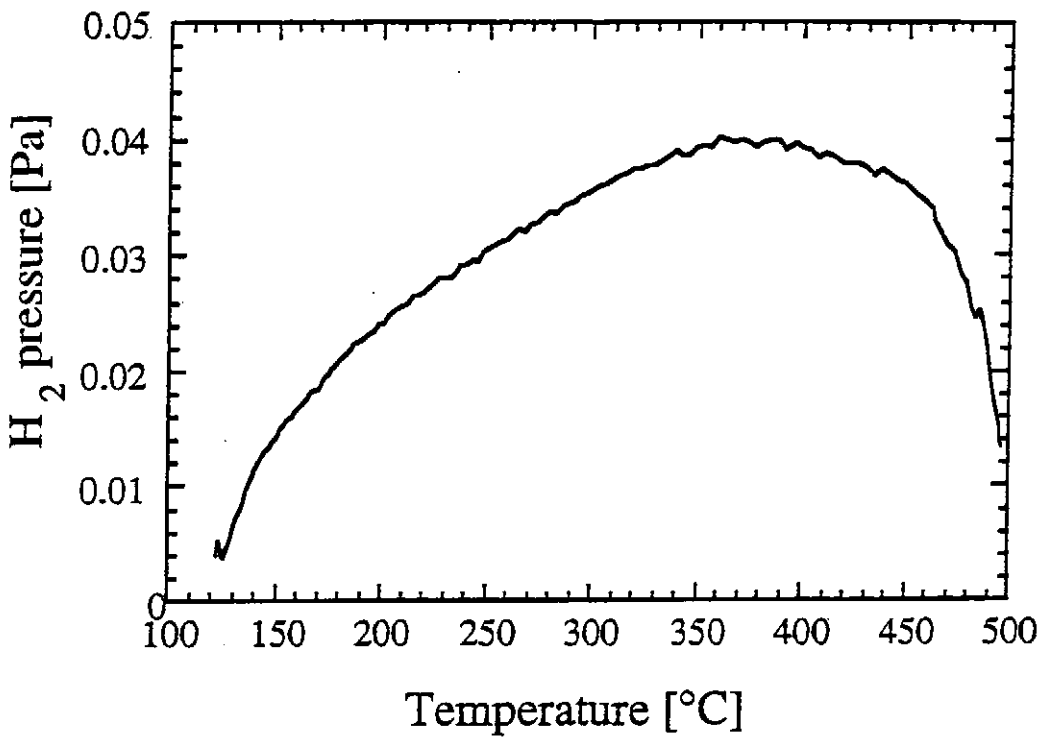

Fig. 8 Hydrogen pressure against liner temperature for same data as Fig. 7

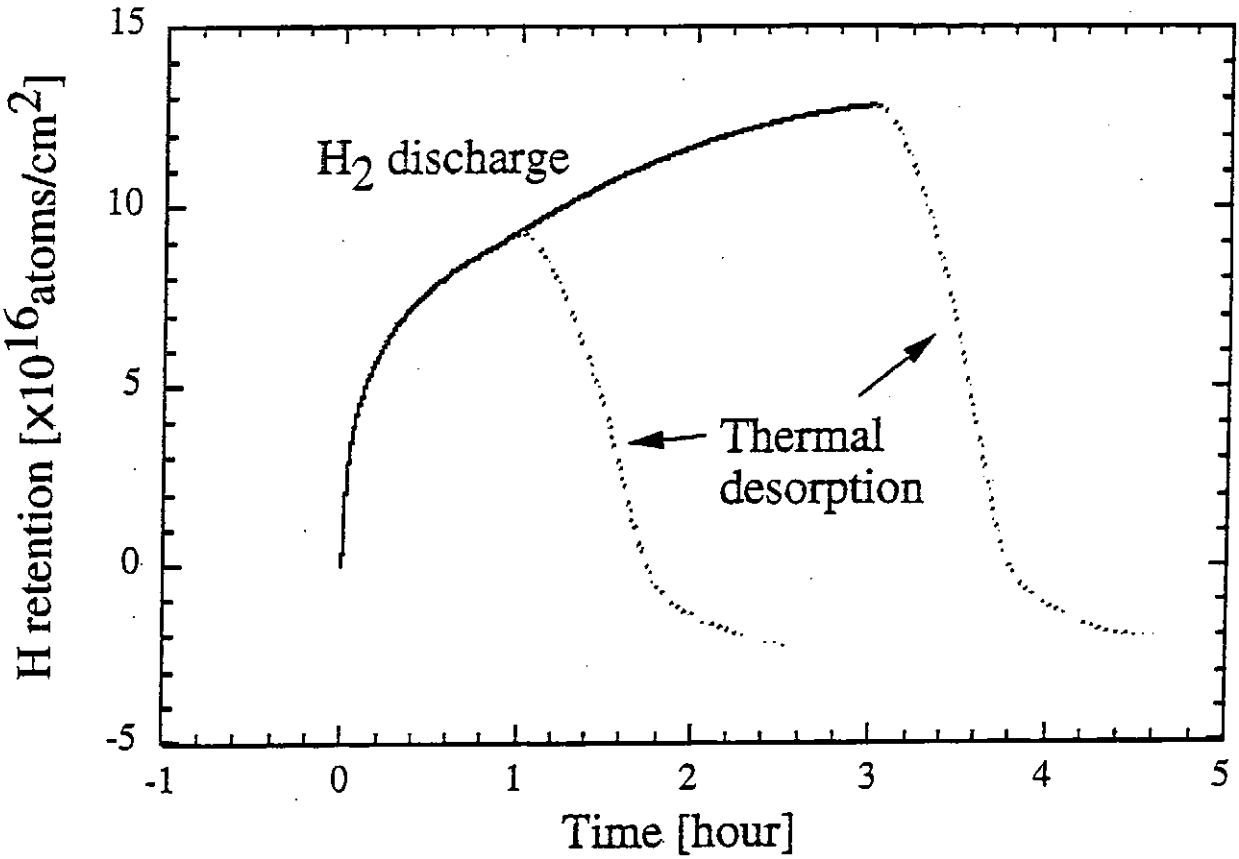

Fig. 9 Hydrogen accumulation during long time H_2 discharge. Dotted lines show decrease of hydrogen atoms during thermal desorption.

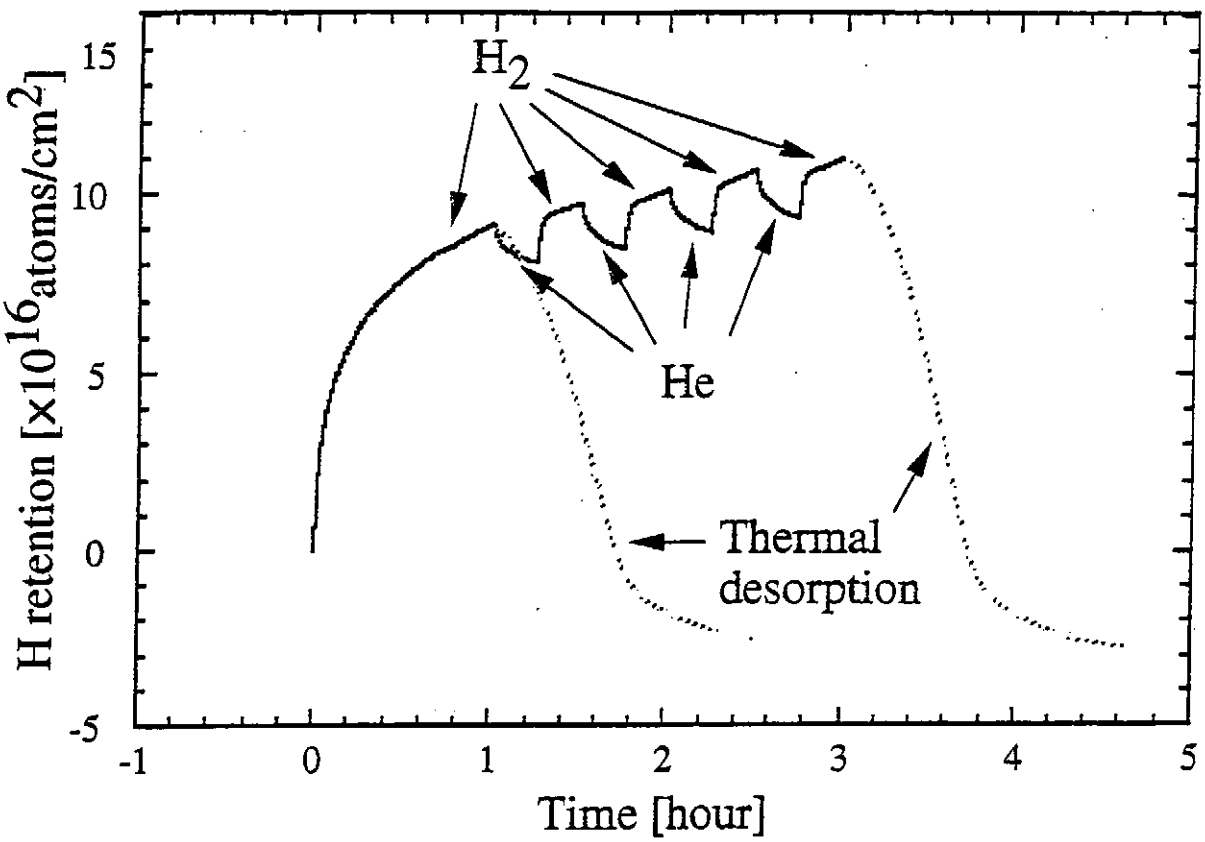

Fig. 10 Time evolution of retained number of H atoms when H2 and He discharges are repeated alternately. The data during thermal desorption are also shown.

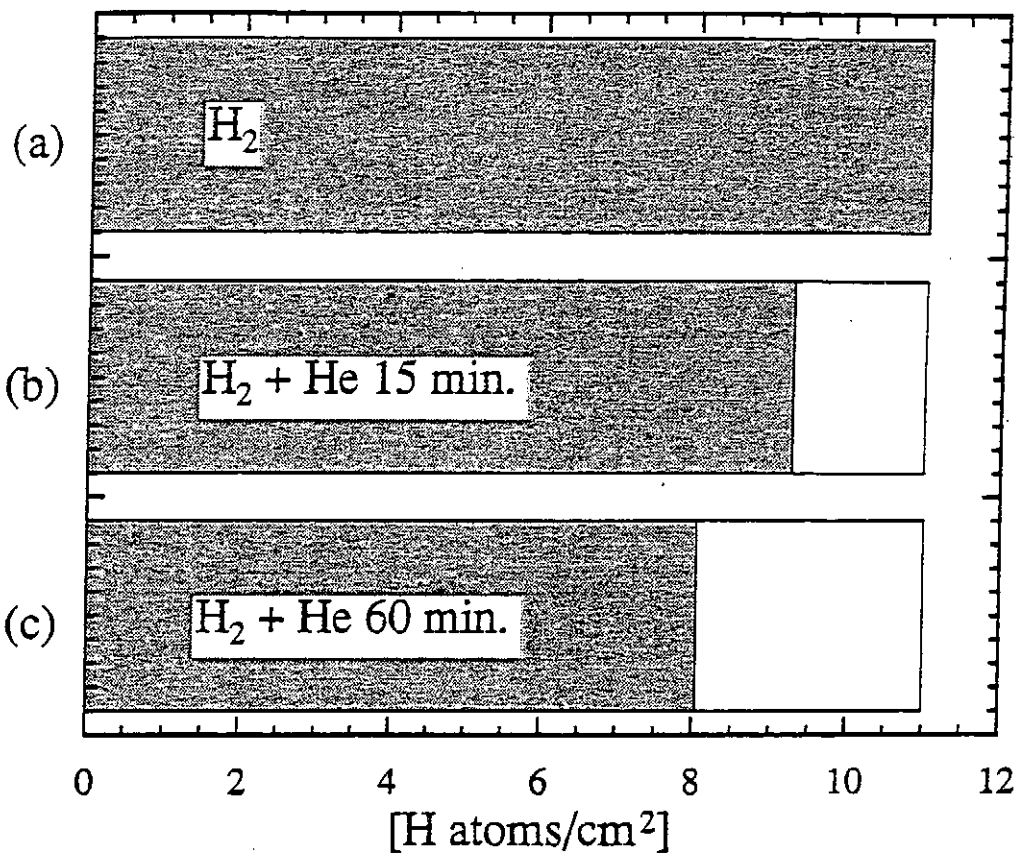

Fig. 11 Number of hydrogen atoms desorbed by heating. The decreased number corresponds to desorbed number of H atoms during the He discharge.

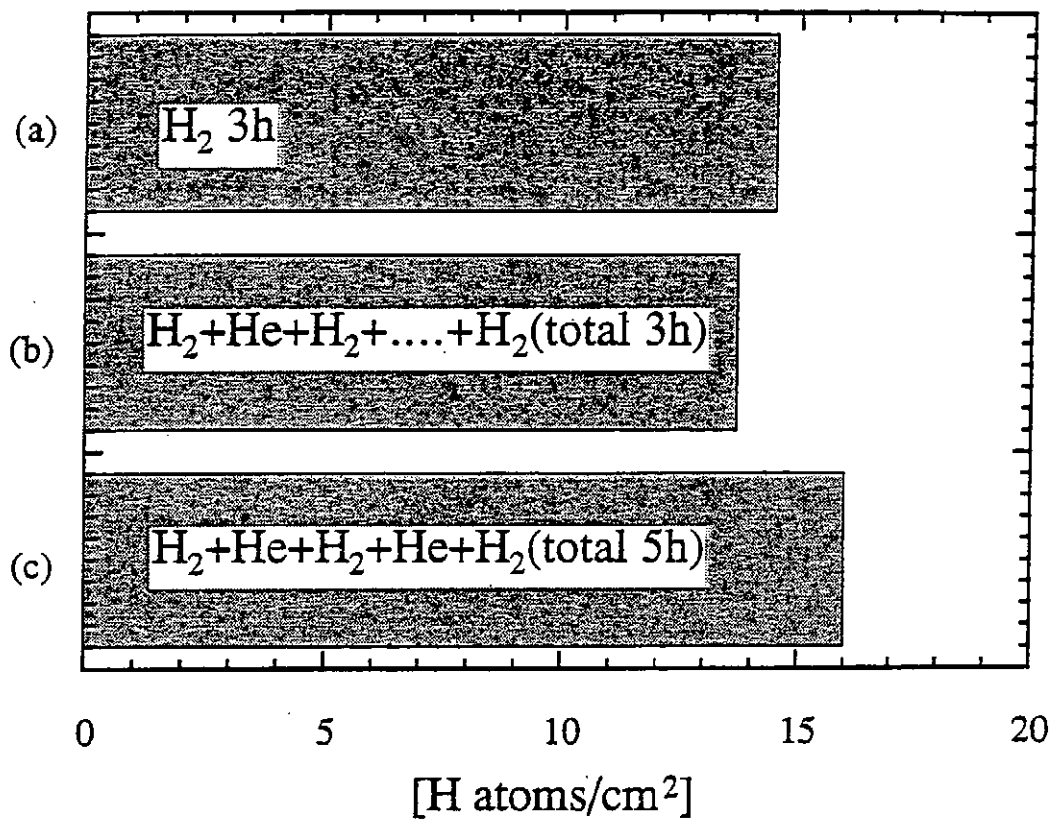

Fig.12 Comparison of desorbed number of H atoms during thermal desorption experiments after (a) 3 hours H_2 discharge(case in Fig.9), (b) 1 hour H_2 and repetition of He/H_2 for 4 times(case in Fig.10), and (c) 1 hour H_2 and repetition of He/H2 for 2 times(1 hour each, total 5 hours, H_2 total 3 hours).

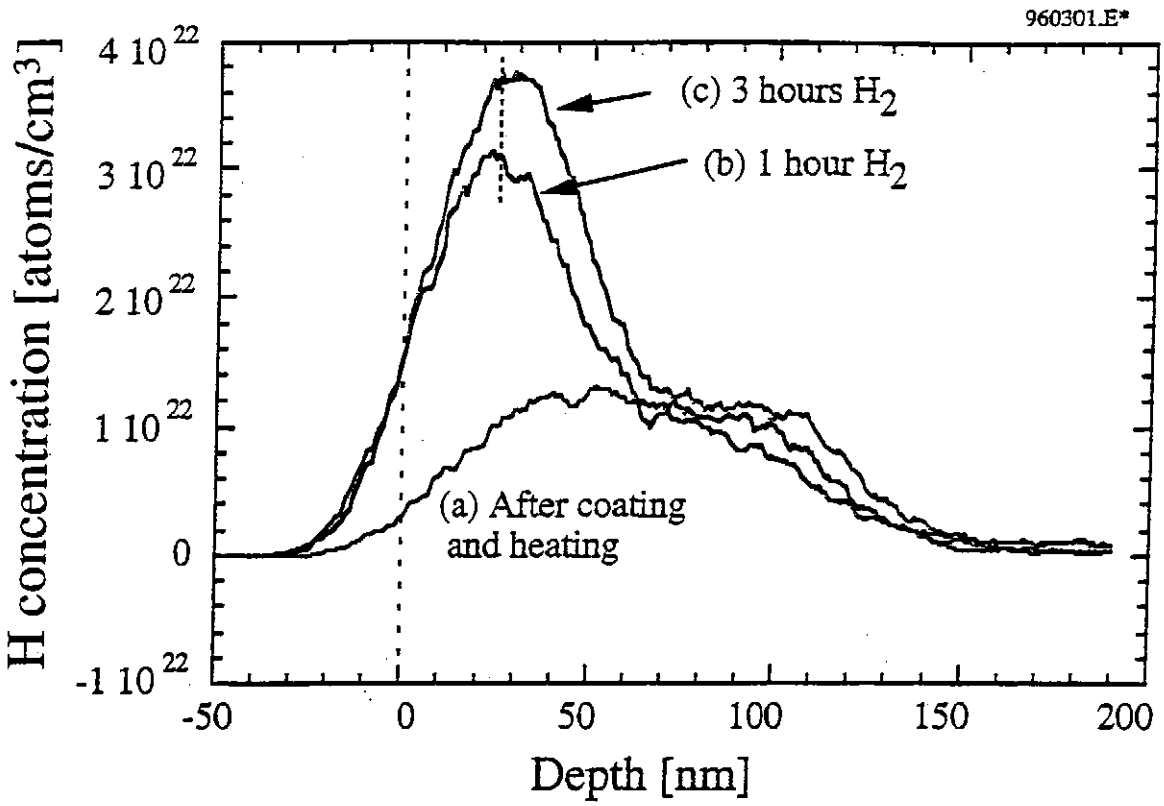

Fig. 13 Depth profile of H atoms measured by ERD

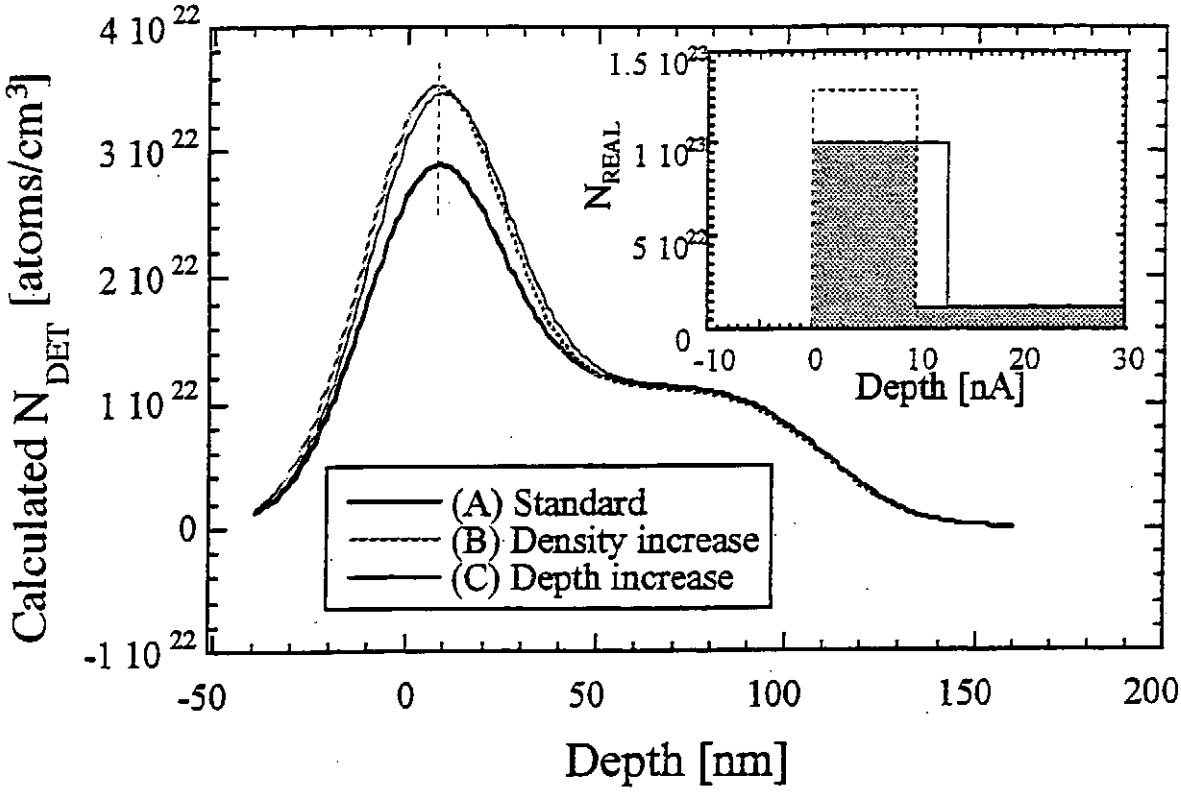

Fig. 14 Calculation of detected profile from real profile. Real profile of squ are type is assumed. The experimental results are reproduced .

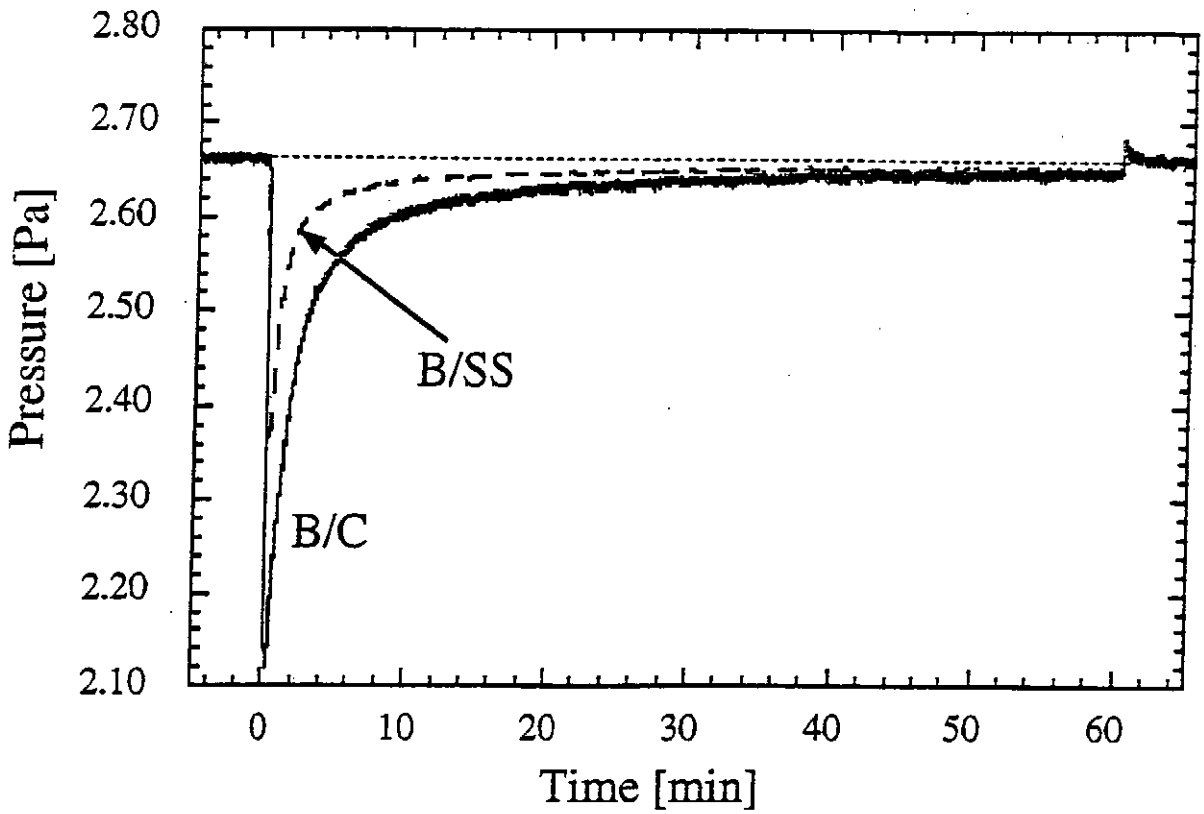

Fig. 15 Time evolution of hydrogen pressure during H_2 discharge with boron film on stainless steel and graphite.

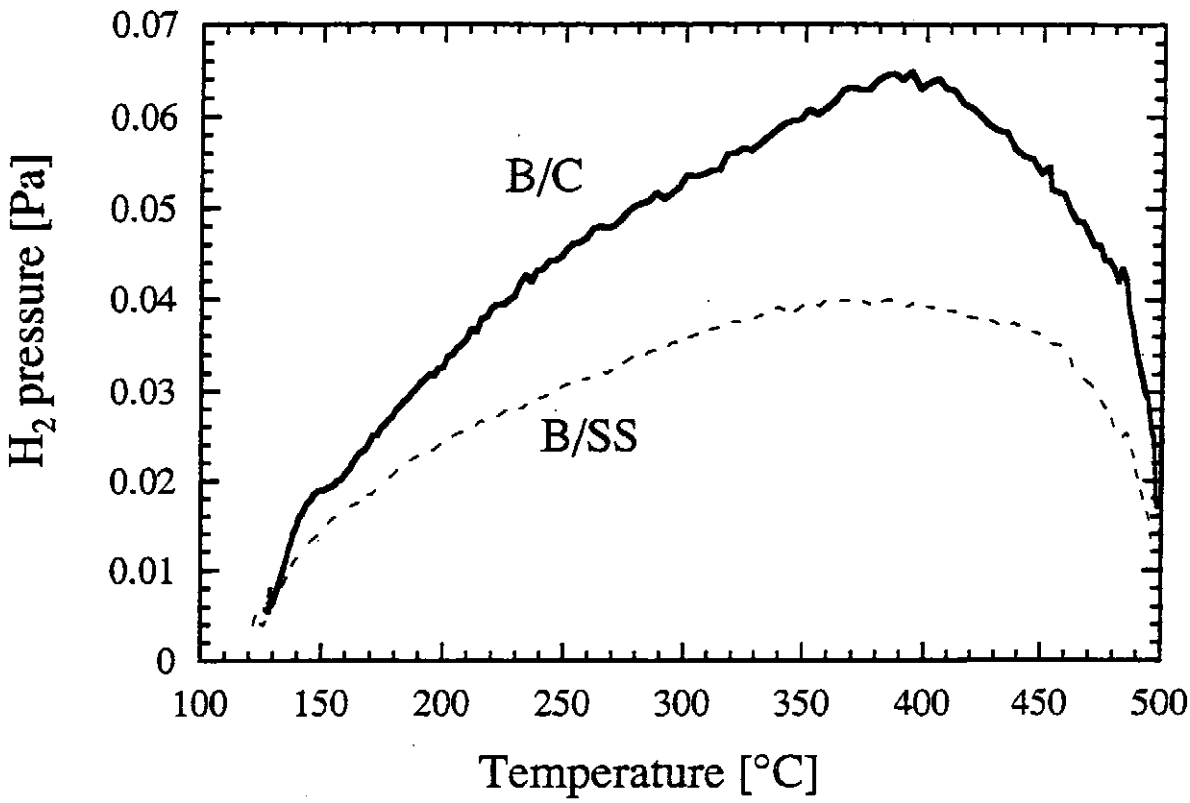

Fig. 16 Time evolution of hydrogen pressure during heating with boron film on stainless steel and graphite.

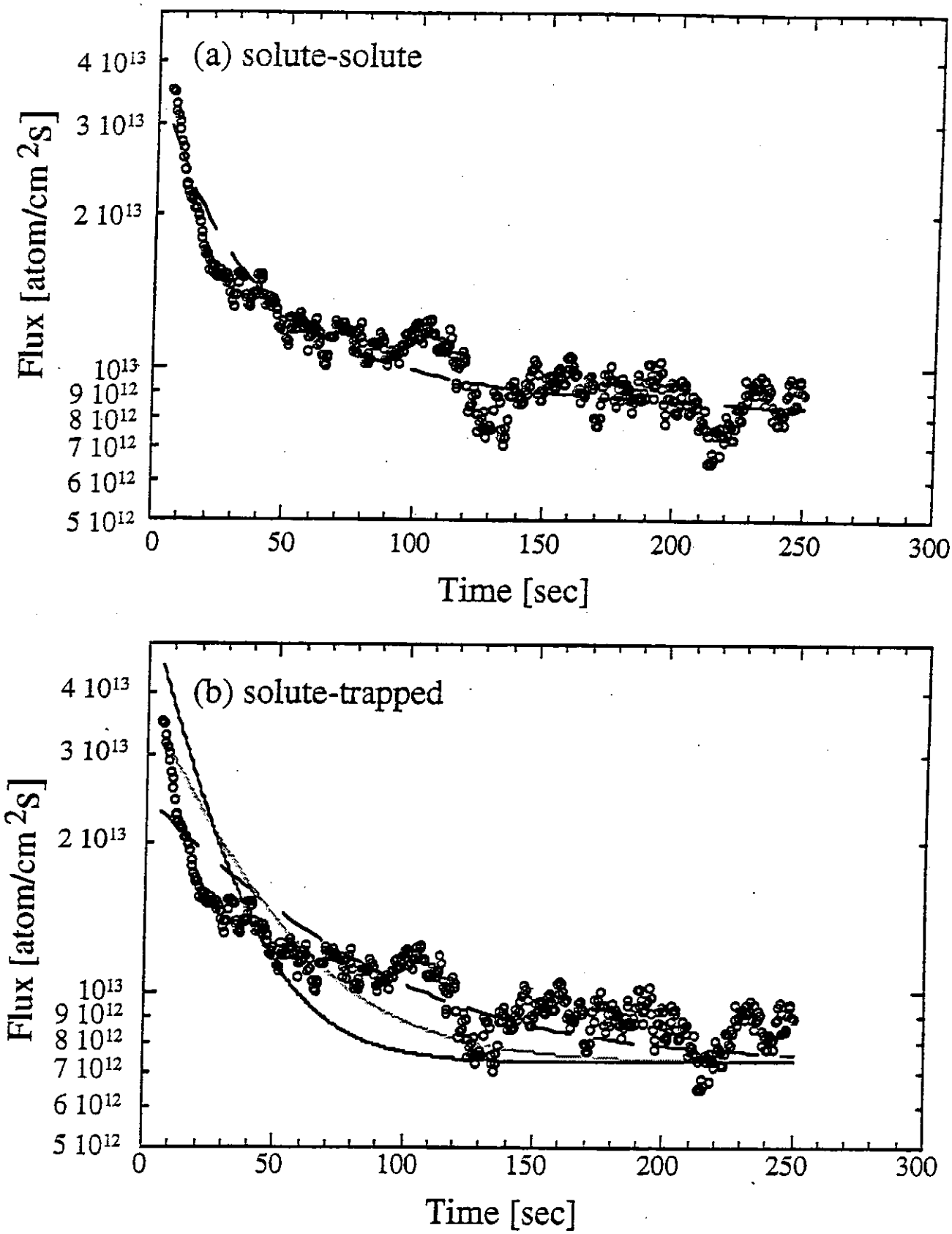

Fig. 17 Hydrogen desorption after termination of hydrogen discharge.
The open circles show experimental results. The lines show calculated results for two extreme cases ;(a) recombination of two solute H atoms is dominant, (b) recombination of solute and trapped H atoms is dominant. The assumption (a) agrees better with the experimental results.

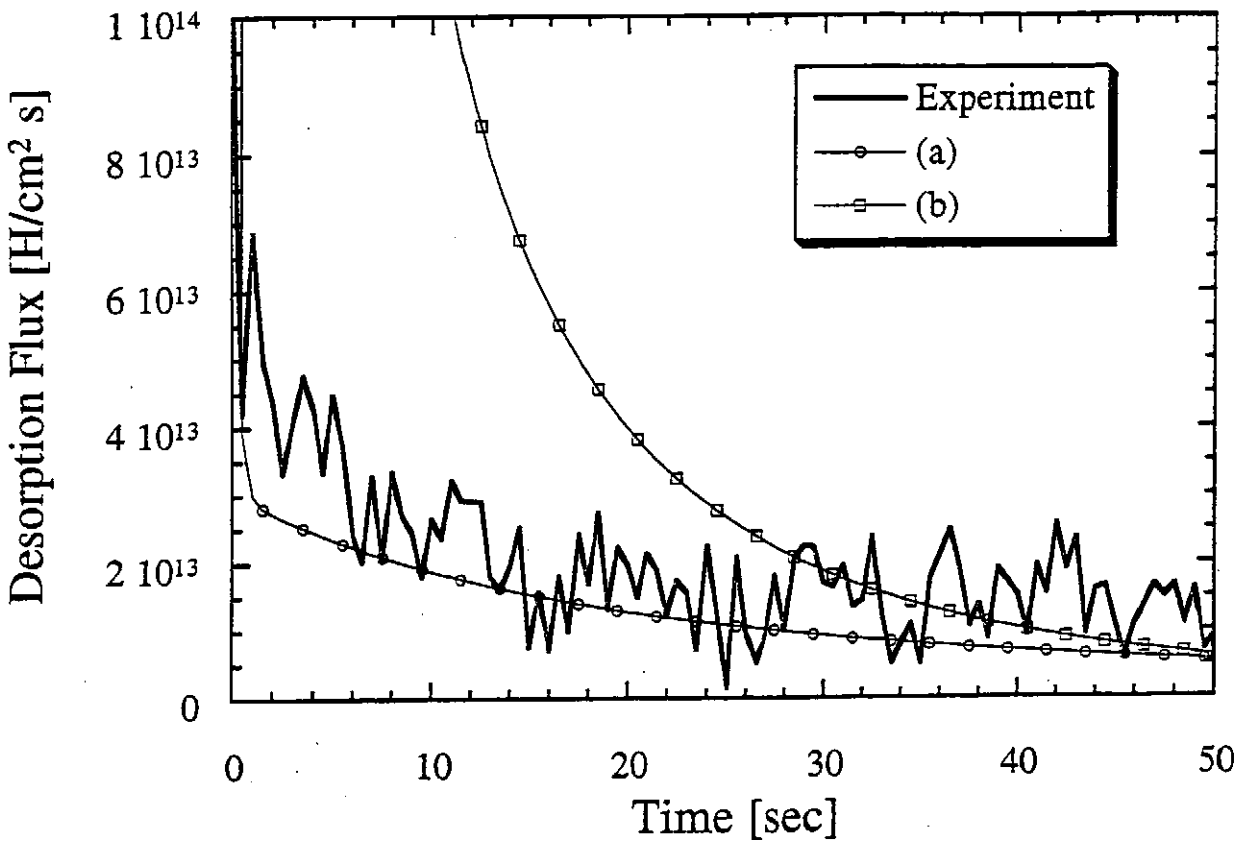

Fig.18 Time evolution of hydrogen pressure after termination of discharge. When the smaller trapping and detrapping probability are used (b) large desorption flux could be observed.

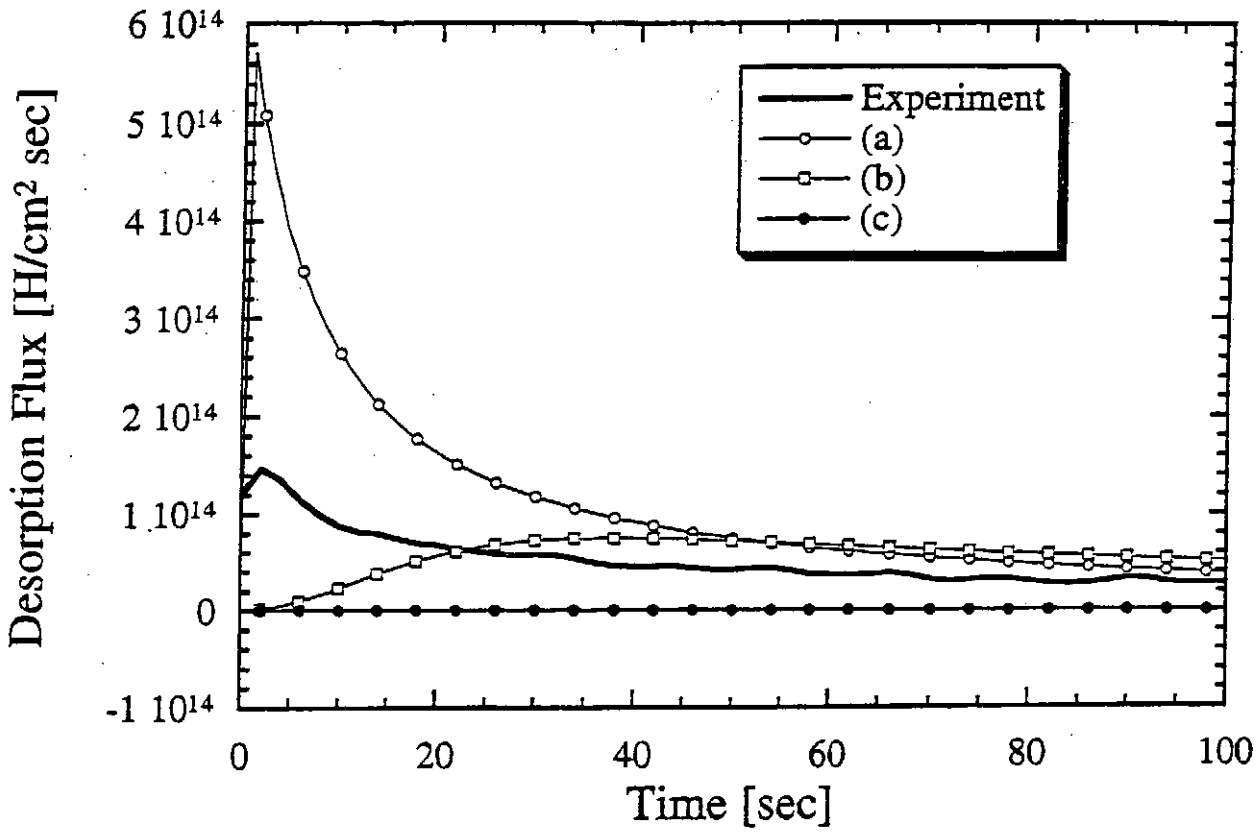

Fig.19 Hydrogen desorption at initial phase of He discharge.
Calculated results are shown for three cases; trapping and detrapping probability is (a) large enough, (b) intermediate, and (c) small enough.

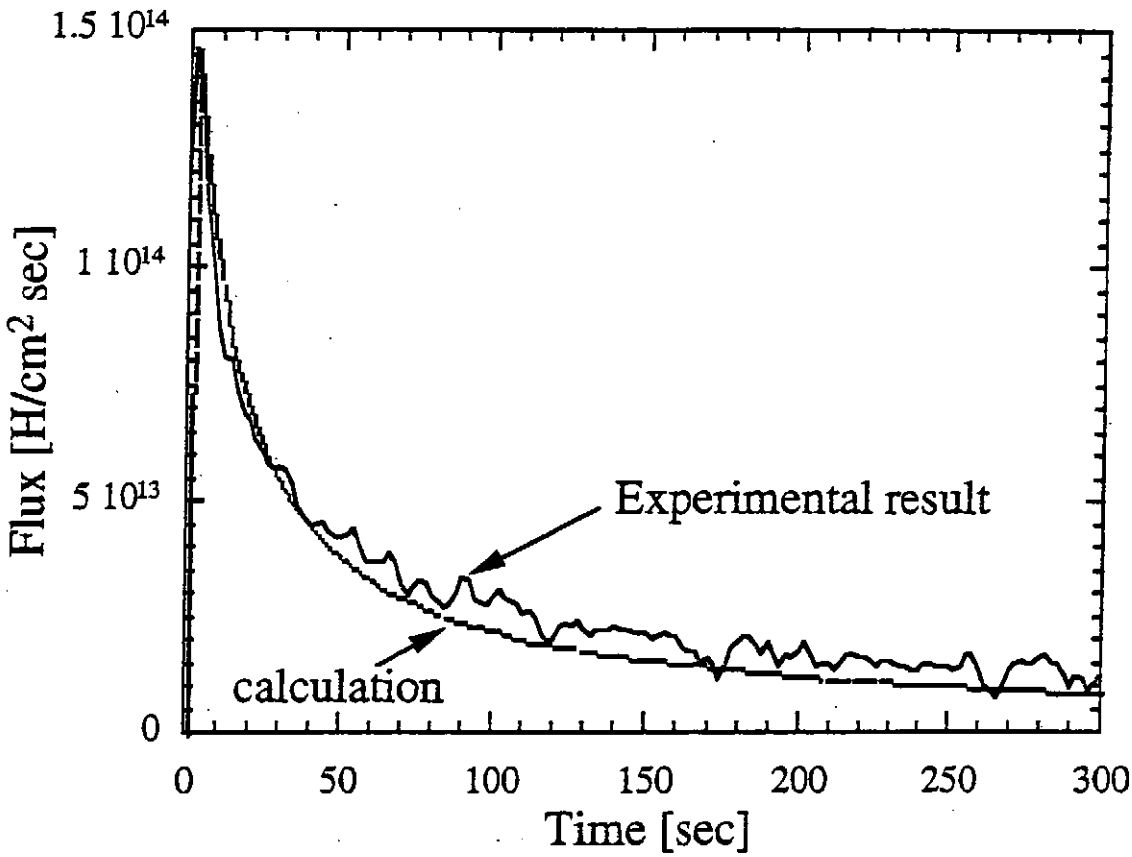

Fig. 20 Hydrogen desorption during He discharge. The calcurated results agree well with the experimental results if the ion induced detrapping cross-section of 5 times smaller than that of hydrogen ion impact.

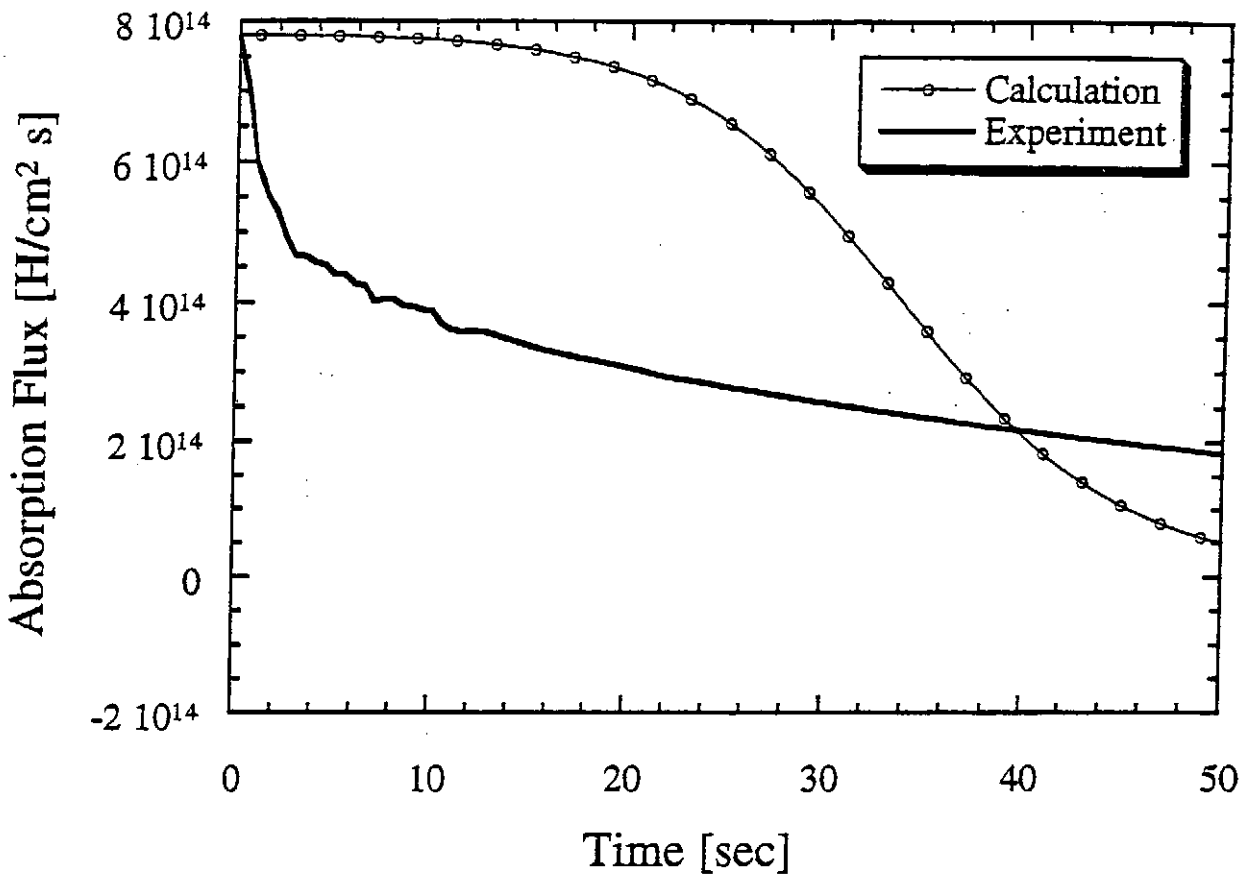

Fig.21 Hydrogen absorption at initial phase of H_2 discharge. Calculated results are shown for the case of large trapping and detraping probability.

Recent Issues of NIFS Series

NIFS-454 S. Saito, Y. Nomura, K. Hirose and Y.H. Ichikawa,
Separatrix Reconnection and Periodic Orbit Annihilation in the Harper Map; Oct. 1996

NIFS-455 K. Ichiguchi, N. Nakajima and M. Okamoto,
Topics on MHD Equilibrium and Stability in Heliotron / Torsatron; Oct. 1996

NIFS-456 G. Kawahara, S. Kida, M. Tanaka and S. Yanase,
Wrap, Tilt and Stretch of Vorticity Lines around a Strong Straight Vortex Tube in a Simple Shear Flow; Oct. 1996

NIFS-457 K. Itoh, S.- I. Itoh, A. Fukuyama and M. Yagi,
Turbulent Transport and Structural Transition in Confined Plasmas; Oct. 1996

NIFS-458 A. Kageyama and T. Sato,
Generation Mechanism of a Dipole Field by a Magnetohydrodynamic Dynamo; Oct. 1996

NIFS-459 K. Araki, J. Mizushima and S. Yanase,
The Non-axisymmetric Instability of the Wide-Gap Spherical Couette Flow; Oct. 1996

NIFS-460 Y. Hamada, A. Fujisawa, H. Iguchi, A. Nishizawa and Y. Kawasumi,
A Tandem Parallel Plate Analyzer; Nov. 1996

NIFS-461 Y. Hamada, A. Nishizawa, Y. Kawasumi, A. Fujisawa, K. Narihara, K. Ida, A. Ejiri, S. Ohdachi, K. Kawahata, K. Toi, K. Sato, T. Seki, H. Iguchi, K. Adachi, S. Hidekuma, S.Hirokura, K. Iwasaki, T. Ido, M. Kojima, J. Koong, R. Kumazawa, H. Kuramoto, T. Minami, I. Nomura, H. Sakakita, M. Sasao, K.N. Sato, T. Tsuzuki, J. Xu, I. Yamada and T. Watari,
Density Fluctuation in JIPP T-IIU Tokamak Plasmas Measured by a Heavy Ion Beam Probe; Nov. 1996

NIFS-462 N. Katsuragawa, H. Hojo and A. Mase,
Simulation Study on Cross Polarization Scattering of Ultrashort-Pulse Electromagnetic Waves; Nov. 1996

NIFS-463 V. Voitsenya, V. Konovalov, O. Motojima, K. Narihara, M. Becker and B. Schunke,
Evaluations of Different Metals for Manufacturing Mirrors of Thomson Scattering System for the LHD Divertor Plasma; Nov. 1996

NIFS-464 M. Pereyaslavets, M. Sato, T. Shimozuma, Y. Takita, H. Idei, S. Kubo, K. Ohkubo and K. Hayashi,
Development and Simulation of RF Components for High Power Millimeter Wave Gyrotrons; Nov. 1996

NIFS-465 V.S. Voitsenya, S. Masuzaki, O. Motojima, N. Noda and N. Ohyabu,
On the Use of CX Atom Analyzer for Study Characteristics of Ion Component in a LHD Divertor Plasma; Dec. 1996

NIFS-466 H. Miura and S. Kida,
Identification of Tubular Vortices in Complex Flows; Dec. 1996

NIFS-467 Y. Takeiri, Y. Oka, M. Osakabe, K. Tsumori, O. Kaneko, T. Takanashi, E. Asano, T. Kawamoto, R. Akiyama and T. Kuroda,
Suppression of Accelerated Electrons in a High-current Large Negative Ion Source; Dec. 1996

NIFS-468 A. Sagara, Y. Hasegawa, K. Tsuzuki, N. Inoue, H. Suzuki, T. Morisaki, N. Noda, O. Motojima, S. Okamura, K. Matsuoka, R. Akiyama, K. Ida, H. Idei, K. Iwasaki, S. Kubo, T. Minami, S. Morita, K. Narihara, T. Ozaki, K. Sato, C. Takahashi, K. Tanaka, K. Toi and I. Yamada,
Real Time Boronization Experiments in CHS and Scaling for LHD; Dec. 1996

NIFS-469 V.L. Vdovin, T.Watari and A. Fukuyama,
3D Maxwell-Vlasov Boundary Value Problem Solution in Stellarator Geometry in Ion Cyclotron Frequency Range (final report); Dec. 1996

NIFS-470 N. Nakajima, M. Yokoyama, M. Okamoto and J. Nührenberg,
Optimization of M=2 Stellarator; Dec. 1996

NIFS-471 A. Fujisawa, H. Iguchi, S. Lee and Y. Hamada,
Effects of Horizontal Injection Angle Displacements on Energy Measurements with Parallel Plate Energy Analyzer; Dec. 1996

NIFS-472 R. Kanno, N. Nakajima, H. Sugama, M. Okamoto and Y. Ogawa,
Effects of Finite-β and Radial Electric Fields on Neoclassical Transport in the Large Helical Device; Jan. 1997

NIFS-473 S. Murakami, N. Nakajima, U. Gasparino and M. Okamoto,
Simulation Study of Radial Electric Field in CHS and LHD; Jan. 1997

NIFS-474 K. Ohkubo, S. Kubo, H. Idei, M. Sato, T. Shimozuma and Y. Takita,
Coupling of Tilting Gaussian Beam with Hybrid Mode in the Corrugated Waveguide; Jan. 1997

NIFS-475 A. Fujisawa, H. Iguchi, S. Lee and Y. Hamada,
Consideration of Fluctuation in Secondary Beam Intensity of Heavy Ion Beam Prove Measurements; Jan. 1997

NIFS-476 Y. Takeiri, M. Osakabe, Y. Oka, K. Tsumori, O. Kaneko, T. Takanashi, E. Asano, T. Kawamoto, R. Akiyama and T. Kuroda,
Long-pulse Operation of a Cesium-Seeded High-Current Large Negative Ion Source; Jan. 1997

NIFS-477 H. Kuramoto, K. Toi, N. Haraki, K. Sato; J. Xu, A. Ejiri, K. Narihara, T. Seki, S. Ohdachi, K. Adati, R. Akiyama, Y. Hamada, S. Hirokura, K. Kawahata and M. Kojima,
Study of Toroidal Current Penetration during Current Ramp in JIPP T-IIU with Fast Response Zeeman Polarimeter; Jan., 1997

NIFS-478 H. Sugama and W. Horton,
Neoclassical Electron and Ion Transport in Toroidally Rotating Plasmas; Jan. 1997

NIFS-479 V.L. Vdovin and I.V. Kamenskij,
3D Electromagnetic Theory of ICRF Multi Port Multi Loop Antenna; Jan. 1997

NIFS-480 W.X. Wang, M. Okamoto, N. Nakajima, S Murakami and N. Ohyabu,
Cooling Effect of Secondary Electrons in the High Temperature Divertor Operation; Feb. 1997

NIFS-481 K. Itoh, S.-I. Itoh, H. Soltwisch and H.R. Koslowski,
Generation of Toroidal Current Sheet at Sawtooth Crash; Feb. 1997

NIFS-482 K. Ichiguchi,
Collisionality Dependence of Mercier Stability in LHD Equilibria with Bootstrap Currents; Feb. 1997

NIFS-483 S. Fujiwara and T. Sato,
Molecular Dynamics Simulations of Structural Formation of a Single Polymer Chain: Bond-orientational Order and Conformational Defects; Feb. 1997

NIFS-484 T. Ohkawa,
Reduction of Turbulence by Sheared Toroidal Flow on a Flux Surface; Feb. 1997

NIFS-485 K. Narihara, K. Toi, Y. Hamada, K. Yamauchi, K. Adachi, I. Yamada, K. N. Sato, K. Kawahata, A. Nishizawa, S. Ohdachi, K. Sato, T. Seki, T. Watari, J. Xu, A. Ejiri, S. Hirokura, K. Ida, Y. Kawasumi, M. Kojima, H. Sakakita, T. Ido, K. Kitachi, J. Koog and H. Kuramoto,
Observation of Dusts by Laser Scattering Method in theJIPPT-IIU Tokamak Mar. 1997

NIFS-486 S. Bazdenkov, T. Sato and The Complexity Simulation Group,
Topological Transformations in Isolated Straight Magnetic Flux Tube; Mar. 1997

NIFS-487 M. Okamoto,
Configuration Studies of LHD Plasmas; Mar. 1997

NIFS-488 A. Fujisawa, H. Iguchi, H. Sanuki, K. Itoh, S. Lee, Y. Hamada, S. Kubo, H. Idei, R. Akiyama, K. Tanaka, T. Minami, K. Ida, S. Nishimura, S. Morita, M. Kojima, S. Hidekuma, S.-I. Itoh, C. Takahashi, N. Inoue, H. Suzuki, S. Okamura and K. Matsuoka,

Dynamic Behavior of Potential in the Plasma Core of the CHS Heliotron/Torsatron; Apr. 1997

NIFS-489 T. Ohkawa,
Pfirsch - Schlüter Diffusion with Anisotropic and Nonuniform Superthermal Ion Pressure; Apr. 1997

NIFS-490 S. Ishiguro and The Complexity Simulation Group,
Formation of Wave-front Pattern Accompanied by Current-driven Electrostatic Ion-cyclotron Instabilities; Apr. 1997

NIFS-491 A. Ejiri, K. Shinohara and K. Kawahata,
An Algorithm to Remove Fringe Jumps and its Application to Microwave Reflectometry; Apr. 1997

NIFS-492 K. Ichiguchi, N. Nakajima, M. Okamoto,
Bootstrap Current in the Large Helical Device with Unbalanced Helical Coil Currents; Apr. 1997

NIFS-493 S. Ishiguro, T. Sato, H. Takamaru and The Complexity Simulation Group,
V-shaped dc Potential Structure Caused by Current-driven Electrostatic Ion-cyclotron Instability; May 1997

NIFS-494 K. Nishimura, R. Horiuchi, T. Sato,
Tilt Stabilization by Energetic Ions Crossing Magnetic Separatrix in Field-Reversed Configuration; June 1997

NIFS-495 T. -H. Watanabe and T. Sato,
Magnetohydrodynamic Approach to the Feedback Instability; July 1997

NIFS-496 K. Itoh, T. Ohkawa, S. -I.Itoh, M. Yagi and A. Fukuyama
Suppression of Plasma Turbulence by Asymmetric Superthermal Ions; July 1997

NIFS-497 T. Takahashi, Y. Tomita, H. Momota and Nikita V. Shabrov,
Collisionless Pitch Angle Scattering of Plasma Ions at the Edge Region of an FRC; July 1997

NIFS-498 M. Tanaka, A.Yu Grosberg, V.S. Pande and T. Tanaka,
Molecular Dynamics and Structure Organization in Strongly-Coupled Chain of Charged Particles; July 1997

NIFS-499 S. Goto and S. Kida,
Direct-interaction Approximation and Reynolds-number Reversed Expansion for a Dynamical System; July 1997

NIFS-500 K. Tsuzuki, N. Inoue, A. Sagara, N. Noda, O. Motojima, T. Mochizuki, T. Hino and T. Yamashina,
Dynamic Behavior of Hydrogen Atoms with a Boronized Wall; July 1997